An Integrated Geothermal Resource Assessment and Techno-Economic Analysis in Presidio County of the Trans-Pecos Region of Texas

Shuvajit Bhattacharya[1], Ken Wisian[1], Bissett Young[1], Malcolm Ross[1,2], Mohamed Khaled[1,3], Rama Chandrudu Arasada[1], Qiqi Wang[1], David Chapman[1], and Aysegul Turan[4]

[1] Bureau of Economic Geology, The University of Texas at Austin, United States

[2] The University of Texas at Austin, United States

[3] Colorado School of Mines, United States (formerly at The University of Texas at Austin)

[4] Institute of Applied Geosciences, Technical University of Darmstadt, Germany

To whom correspondence should be addressed. Emails:

shuvajit.bhattacharya@beg.utexas.edu; ken.wisian@beg.utexas.edu

An Integrated Geothermal Resource Assessment and Techno-Economic Analysis in Presidio County of the Trans-Pecos Region of Texas

Shuvajit Bhattacharya[1], Ken Wisian[1], Bissett Young[1], Malcolm Ross[1,2], Mohamed Khaled[1,3], Rama Chandrudu Arasada[1], Qiqi Wang[1], David Chapman[1], and Aysegul Turan[4]

[1] Bureau of Economic Geology, The University of Texas at Austin, United States

[2] The University of Texas at Austin, United States

[3] Colorado School of Mines, United States (formerly at The University of Texas at Austin)

[4] Institute of Applied Geosciences, Technical University of Darmstadt, Germany

Shuvajit.bhattacharya@beg.utexas.edu

ABSTRACT

Presidio County of the Trans-Pecos region of Texas has substantial, undeveloped geothermal resources. We conduct a thorough, multi-scale characterization of geothermal resources and assess techno-economics for power generation and direct use facilities. We integrate surface geology, high-resolution gravity, borehole geophysical logs, and core data for subsurface characterization and carry out detailed techno-economics, considering enhanced geothermal systems (EGS) and closed-loop geothermal systems (CLGS) technologies. Techno-economic analysis shows that the geothermal resource development in Presidio County could be economically viable for a wide range of project scenarios for power generation and direct use, with a project lifetime of 20-30 years. However, the economic outlook of geothermal project developments in the study area are varied and range from poor to excellent, depending on the target location, reservoir depth, temperature, completion technologies, and local demand for utilization.

The Border region of the study area has the best quality geothermal resources. The geothermal gradient in the Border region is significantly high (~47°C/km), indicating a shallow drilling depth to reach a target temperature. The Interior Region has a cooler geothermal gradient of ~29°C/km. Not much information is available from the Big Bend Region, regarding the deep geothermal potential. New higher resolution geophysical surveys and drilling new wells can help improve our understanding of the local geology and available geothermal resources in the study area.

INTRODUCTION

Geothermal energy can provide 24/7 baseload energy; it is expected to only increase its popularity due to its multitude of utilization, modularity, and capability to meet the demands of grid capacity, compared to many other renewable energy sources. There has been a significant increase in the exploration and pilot demonstrations of geothermal energy beyond traditional district heating due to innovations and investments in new-edge drilling and completion technologies, including single/multi-well closed-loop and horizontal well drilling and stimulation of "Hot dry rock" (HDR). Energy storage is a new addition to the geothermal portfolio that can provide baseload power when other renewable energies like solar/wind plants are not operational.

Presidio County in the Trans-Pecos region of Texas has long been considered to have geothermal potential (**Figure 1**). Presidio County of Texas borders Mexico. It is located west of the Big Bend National Park. The overall study area has a vast land, with a history of renewable energy projects, international trade and transportation, and potential of government incentives. However, the population is very small (6,131, as of United States Census Bureau, 2020), with limited entrepreneurship and water supplies. The objective of this study is to generate an up-to-

date foundational knowledge in subsurface geology and estimate geothermal resources in the study area, and how that impacts techno-economics of various kinds of geothermal energy utilization. Geothermal energy can be used as a commodity for power generation (thereby expanding grid capacity) and various kinds of direct use, while decarbonizing the grid.

Subsurface geology of Presidio County is not well understood due to its complex geologic features, the presence of multiple basins, varying geothermal gradients, and a lack of deep borehole investigations. Limited geologic studies have been conducted in the overall Trans-Pecos region of Texas (Lonsdale, 1940; Dietrich, 1965; Goldich, 1949; Kopp, 1977; Mraz, 1980; Parry, 1857). Unlike many other areas in Texas, this study region has not yielded hydrocarbons despite several drilling attempts. Recently, Helios Energy completed two vertical wildcat wells in the Cretaceous Ojinaga Shale, at an approximate depth of 4,800 feet (1.5 km), with some flow tests.

Over the years, there have been several geothermal studies in Trans-Pecos region of Texas, specifically, Presidio County (Kopp, 1977; O'Donnell et al., 2001; Lear et al, 2016). However, there are not many published studies on deep geothermal ('geothermal anywhere') potential and detailed techno-economics for both power generation and direct use. Most recently, Wisian et al. (2024) produced a preliminary, non-peer-reviewed project report for the Presidio Municipal Development District on the geothermal potential in Presidio County. Our current study is an extension of that but more enhanced from various geologic and geophysical aspects, including new data and interpretations of gravity, core, basement, faults, and fractures.

This study integrates temperature, reservoir, faults, and fracture information from various kinds of geologic and geophysical data for subsurface analysis. It then uses subsurface parameters to develop various techno-economics scenarios for either power generation or various kinds of direct use (agricultural processing, absorption chiller, etc.).

We expect that the outcome of this study will empower the local government, residents, industry, and other stakeholders to leverage the significant economic potential of geothermal energy development in the study area. It will also help prospective developers understand the resources better and evaluate their proposals effectively. In addition, this study will establish a workflow for analyzing the feasibility of geothermal energy exploration and utilization in regions that lack data and have complex geologic conditions. In this context, we broadly define geothermal power to include electricity generation, and direct use, such as heating and cooling, industrial processes, agricultural and aquaculture heating, etc.

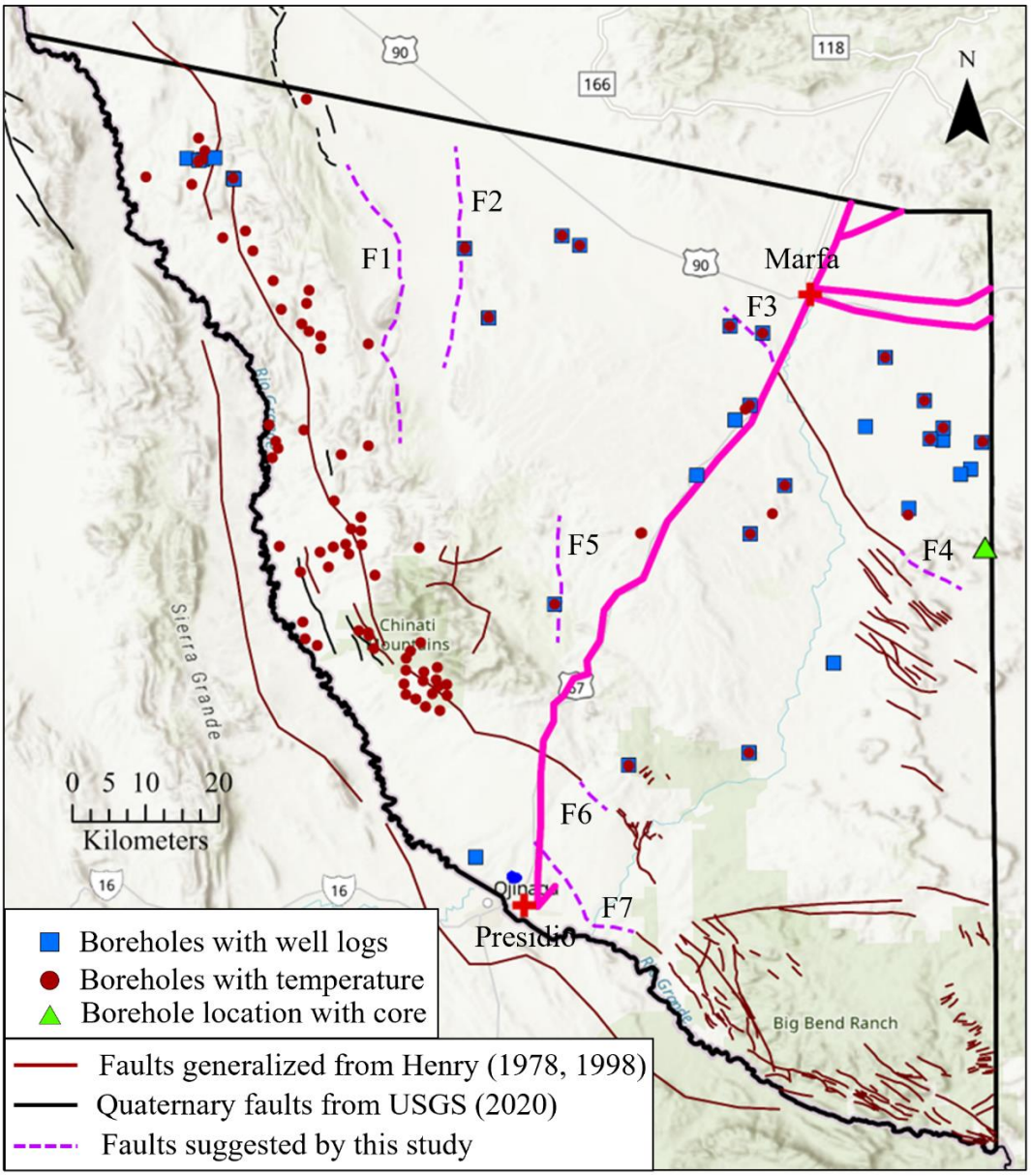

Figure 1. The location of the study area in Presidio County in SW Texas. Filled circles in brown indicate boreholes with temperature data, blue squares indicate wells with geophysical logs, and green triangle indicates deep well with core. Brown, black, and purple (dash) lines show interpreted faults from the literature, USGS, and this study. Thick magenta line, connecting Marfa to Presidio indicates the ERCOT grid transmission line.

KEY ASPECTS OF CURRENT GEOTHERMAL DEVELOPMENT TECHNOLOGIES

We can classify geothermal power systems into two main types: hydrothermal (also known as conventional geothermal) and hot dry rock (also referred to as HDR or Geothermal Anywhere). The terminology surrounding “Geothermal Anywhere” approaches can be inconsistent and varies widely. Commonly used terms include Advanced Geothermal Systems (AGS), Enhanced Geothermal Systems (EGS), and Closed Loop Geothermal Systems (CLGS). For clarity, we use the broad terms " Geothermal Anywhere " and "hot dry rock" interchangeably.

Hydrothermal systems are a well-established technology deployed worldwide (US, Turkey, Indonesia, etc.). They harness naturally occurring steam or hot brine from the Earth to drive a turbine or generator, producing electricity.

On the other hand, "Geothermal Anywhere" leverages an engineered fluid system to extract heat from rock. This concept has been long desired and is now becoming feasible due to various technological advancements. The growing need to expand grid capacity and decarbonize electricity production has made it practical and economically viable to extract heat directly from rock. We expect these new-generation "Geothermal Anywhere" approaches becoming more successful than conventional hydrothermal projects.

The direct use of geothermal heat is significantly more abundant (due to a lower temperature threshold) and more efficient, typically achieving over 80% efficiency. This is in comparison to generating power, which generally yields less than 20% efficiency. Direct use can include heating and cooling, agriculture, aquaculture, etc.

An associated technology is a "ground source heat pump." Heat pumps are fairly widespread in the U.S. (mostly in the northern regions), particularly in single-home and

neighborhood settings. These direct-use technologies are well-developed and can be implemented quickly.

Finally, thermal or mechanical energy storage of energy in the Earth is another rapidly advancing technology, with high efficiency. Energy can be stored in rock formations through pressure or thermal changes. We have not considered this technology in our study.

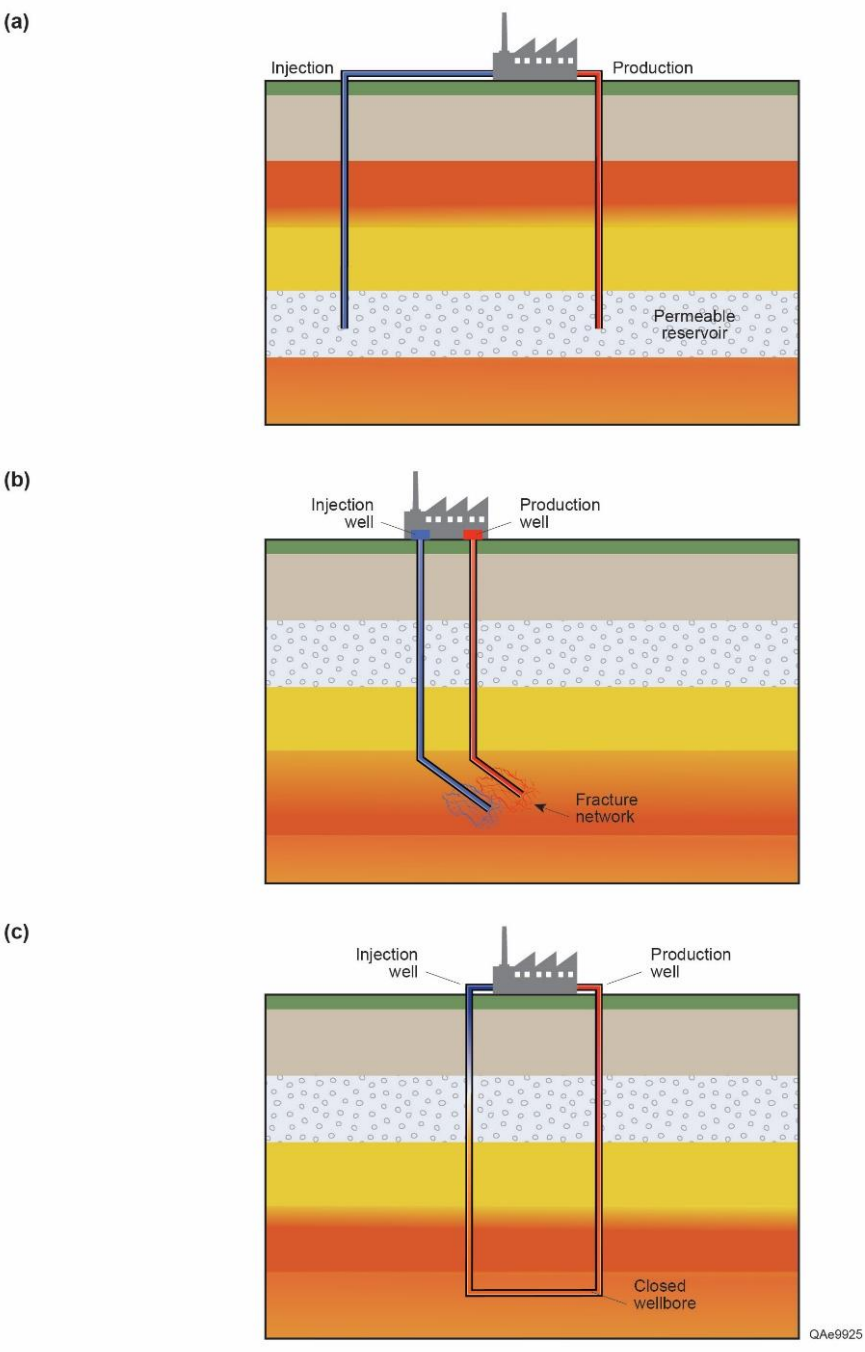

Figure 2. Schematic diagrams of (a) a "conventional" hydrothermal system, (b) Enhanced Geothermal System (EGS), and (c) A closed-loop geothermal system (CLGS) or Advanced Geothermal System (AGS).

SUBSURFACE GEOLOGIC CHARACTERIZATION

Regional Geology

We divide the entire study area into three regions based on the regional geology and thermal patterns: “Border,” “Interior,” and “Big Bend” (**Figure 3**). The Border Region is located along the US/Mexico border, and the Interior region is in the inner majority of the study area, whereas Big Bend is in the SE corner. The study area contains multiple basins: Valentine Basin (towards the North), Marfa Basin (towards East-Central), Presidio Bolson, and Redford Bolson (towards Southwest). Presidio Bolson and Redford Bolson are at the border region. These bolsons are located in grabens trending NNW along the border region of the study area, filled with Quaternary sediment deposits (Mraz and Keller, 1980). The Presidio Graben is bounded in the east by the Sierra Vieja, the Chinati Mountains, and the Bofecillos Mountains, and on the west it is bounded by the Chihuahua Tectonic Belt in the State of Chihuahua, Mexico (Mraz and Keller, 1980). These bolsons were formed by the Tertiary normal faulting (Groat, 1972). There are several extensional faults oriented along NW/NNW.

The Precambrian basement is heterogeneous; it comprises of arkosic sandstone, granite, rhyolite, quartzite, etc. (Stoeser et al., 1992). The deepest sedimentary formation is thought to be the Bliss sandstone, which unconformably overlies the Precambrian basement. The Ellenburger carbonates (equivalent of El Paso Group) overlie the Bliss sandstones. Apart from Ellenburger carbonates, other formations in the Paleozoic-Mesozoic era include Fusselman, Montoya, Shafter, and Presidio formations. Basin and Range extensional faulting and igneous activities dominated during the Tertiary era in the study area. Volcanic centers in the overall Trans-Pecos region include several localized accumulations of lavas, ash flow, and intrusions (Walton and Henry, 1978). Although just outside our specific study area, the Solitario in neighboring Brewster County of Texas is a Tertiary-aged circular laccolithic dome and caldera in southern Trans-Pecos region

(Henry and Muehlburger, 1996). It is considered among the world's largest laccoliths. Please see Stoeser et al. (1992), Henry and Muehlberger (1996), and Frelinger (2015) for more details on regional geology of the study area. **Figure 4** shows simplified lithostratigraphy in the study area.

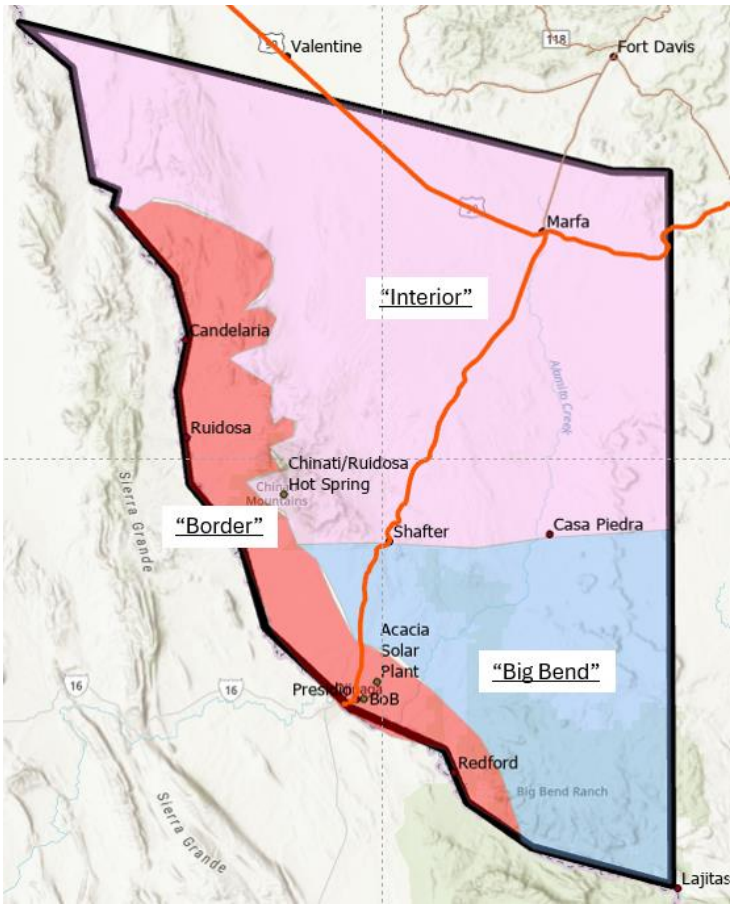

Figure 3. Border, Interior, and Big Bend regions in the study area. The boundaries between these regions are approximate (Wisian et al., 2024).

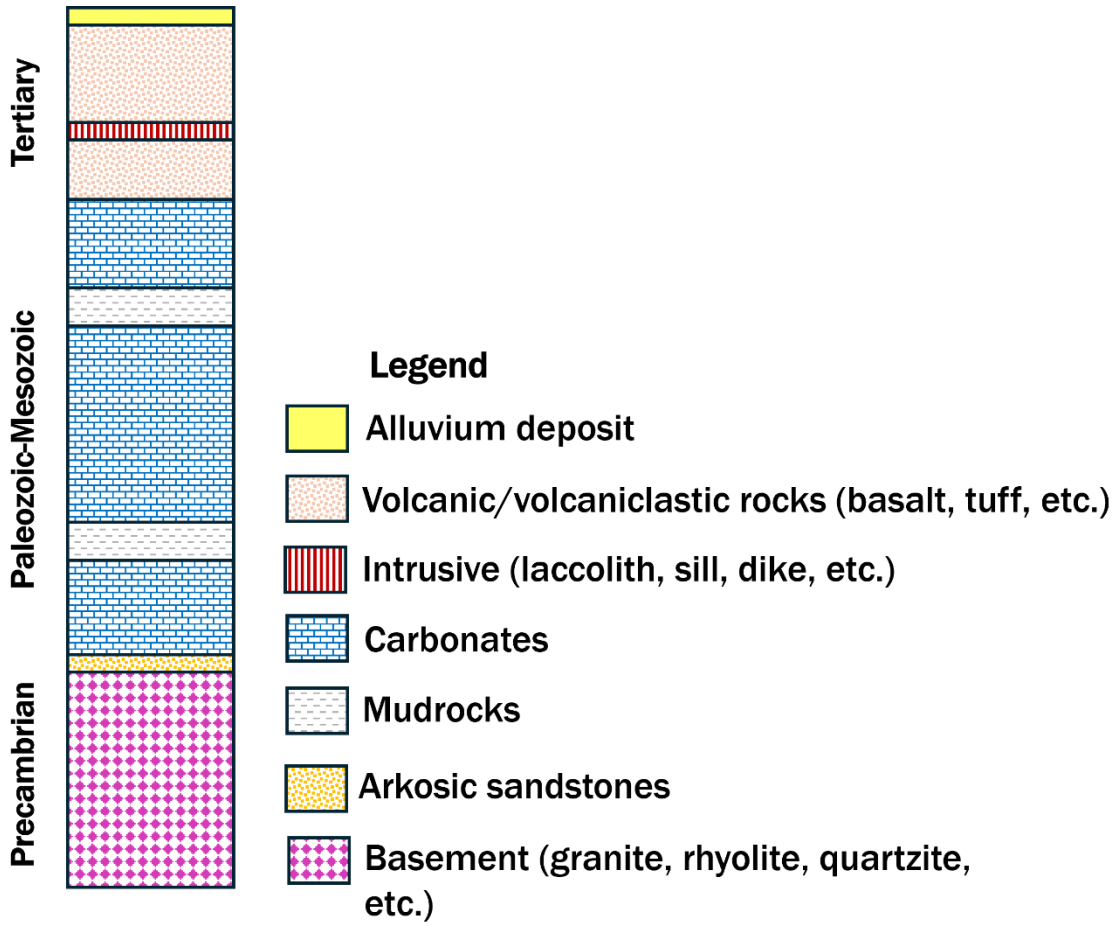

Figure 4. Simplified litho-stratigraphy of the study area (approximate scale)

AVAILABLE DATA

In this study, we integrated a swath of multi-scale geologic and geophysical data for subsurface characterization: potential field data (high-resolution gravity), mud logs, petrophysical logs from 14 deep wells, core from a deep well, surface geology maps, and published literature.

We used temperature data from 120 unique bottom hole temperature (BHT) samples from 101 wells in the Presidio County. These data came from many sources, including Southern Methodist University (Blackwell et al., 2011), Bureau of Economic Geology (BEG) well database, and Standard and Poor's (S&P) Enerdeq Browser.

We also licensed a high-resolution gravity data from Getech. The high-resolution gravity data helped to understand the geology of the subsurface in more detail than the publicly available gravity data in contemporaneous US and Texas (Hittleman et al., 1994; Kucks, 1999; Bankey, 2006). Note that high-resolution magnetic and radiometric surveys in the overall study area may become available under the USGS Earth Mapping Resources Initiative (MRI) program in the future (https://www.usgs.gov/earth-mapping-resources-initiative-earth-mri).

Most of the wells with petrophysical logs are present in the Border Region and Interior Region. We did not have access to information about any deep wells from the Big Bend Region, which adds uncertainties to the results. We also studied the 4-in. (10-cm)-diameter core from Gulf Mitchell Bros. State No. 1 well from the Interior Region of Presidio County. The depth interval of the cored Ellenburger section is 15,266 ft (4,653 m) to 15,984 ft (4,872 m).

METHODS FOR INTEGRATED SUBSURFACE INTERPRETATIONS

We applied a multi-scale, integrated approach to characterize the geothermal resource within the study area. Each data type required a different processing approach; in some cases, new data acquisition as well, all of which were integrated at the end to quantify the geothermal resource and techno-economics.

Gravity data analysis

For gravity data, we used descriptive and quantitative approaches (inversion of high-resolution gravity data) to determine gravity-highs (mountains, upthrown fault blocks, etc.) and gravity-lows (basins, down-thrown fault blocks) and the depth to the top of the Precambrian

basement. We also conduct forward modeling of gravity data to build geologic cross-section across the entire study area.

Core, well log, and mud log analysis

We analyze available well logs, mud logs, and core data to interpret lithology and reservoir properties, such as porosity. For fracture analysis, we identify the types of fractures present and their orientation from the Gulf Mitchell Bros. State No. 1 well. No fracture information had been collected in the well when it was drilled. The core was not oriented during drilling, and it was broken into several pieces that could not be fit back together. Therefore, it was not possible to measure fracture orientations from the core. There was no image log available from this well.

Temperature data analysis

The compiled BHT data is relatively well-distributed across the county from west to east; however, it is notably absent in the southeastern region, particularly near Big Bend (**Figure 5**). While BHTs tend to be a "noisy" data source, they are generally considered valuable indicators of temperature if the samples are used collectively to understand broad temperature pattern in the subsurface. Additional methods for measuring temperature may include fiber-optic distributed temperature sensing and Curie point depth data.

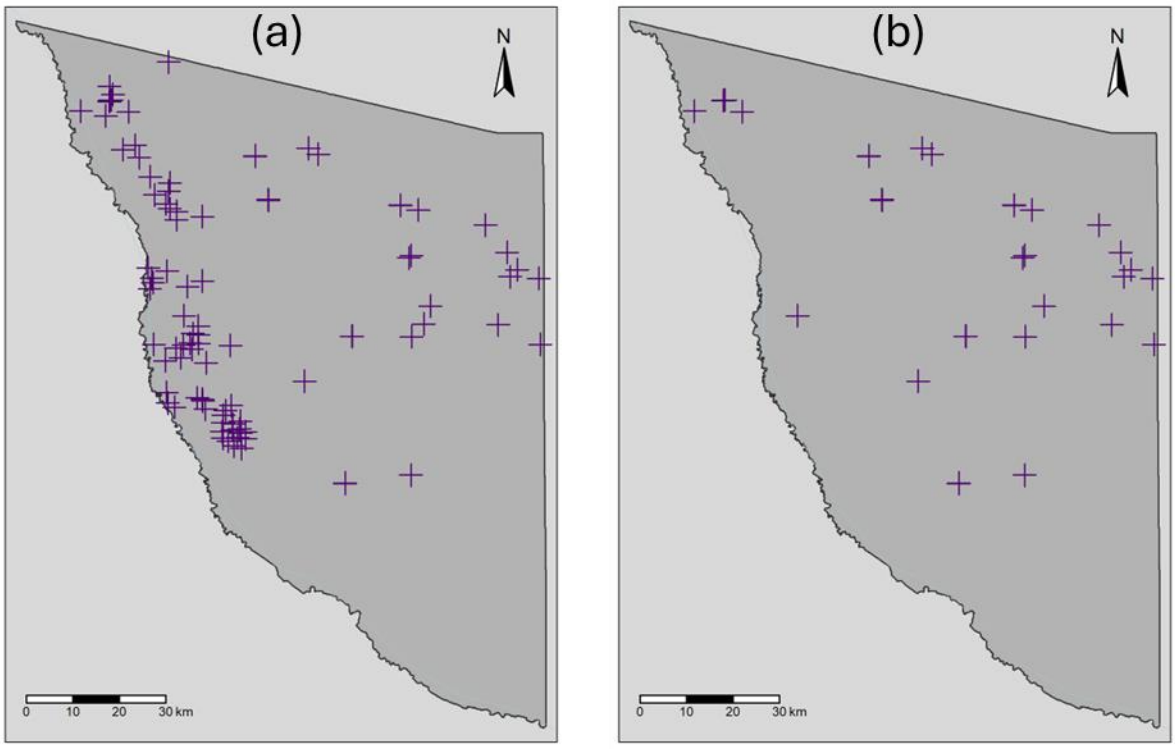

Figure 5. The locations of wells with temperature data in the study area. 5**a** is all data points (affected by shallow spurious data), **5b** filtered data with a depth greater than 1,000 ft (after removal of shallow samples, affected by groundwater movement.

Since raw BHT data does not represent the true (equilibrium) temperature of the rock, we applied Harrison corrections method to this dataset. There are several methods for correcting Bottom Hole Temperatures (BHT), each designed to calibrate BHT to the equilibrium temperature specific to particular study areas. However, these methods may not be universally reliable. In this study, we follow previous geothermal research conducted in Texas and apply a modified version of the Harrison correction (Harrison, 1983; Blackwell, 2011; Batir and Richards, 2020), which is widely considered an industry standard.

$$T_c(℃) = (T_m - T_a) - 16.512 + 0.0183d - 0.00000234d^2$$

where "d" represents depth in meters, "T_m" is the measured temperature, and "T_a" is the average ambient temperature for the area. This equation is applicable to BHTs at depths less than 3.8 km. For depths greater than 3.8 km, we need to apply a constant shift of +19.1°C.

Apart from Harrison's correction, we also build a best-fit temperature model using lithology, lithology-specific thermal conductivity, and depth range of the dominant rock types. This method generates a temperature model that can be extrapolated to the target depth.

METHODS FOR TECHNO-ECONOMICS

After we analyze and compile the subsurface information, we conduct techno-economic assessments of the study area, considering a multitude of options and utilizations, using two different options: Heat in Place - Resource Assessment (HIP-RA) and GEOthermal energy for Production of Heat and electricity ('IR') Economically Simulated (GEOPHIRES) tool from National Renewable Energy Laboratory.

Heat in Place - Resource Assessment (HIP-RA) approach

"Heat In Place - Resource Assessment (HIP-RA)" (Muffler and Cataldi, 1978; Garg and Comb, 2011) approach, originally developed by USGS, offers a high-level overview of the geothermal resources of a given reservoir. This volumetric-based analysis approach outputs the amount of producible heat in the reservoir and the amount of producible electricity. Both the heat and producible electricity are expressed per unit volume. The HIP-RA utilizes a few input variables, such as reservoir area, reservoir thickness, reservoir porosity, reservoir temperature, rejection temperature, and volumetric heat capacity (depending on heat capacity and density of fluid and rock matrix). However, the results from this approach may have high uncertainties.

To address the inherent lack of accuracy, HIP-RA analyses frequently employ Monte Carlo (MC) simulations, in which 1,000s of simulations can be run, with randomized and reasonable values of the input variables. In this study, we iterated MC simulations 2,500 times.

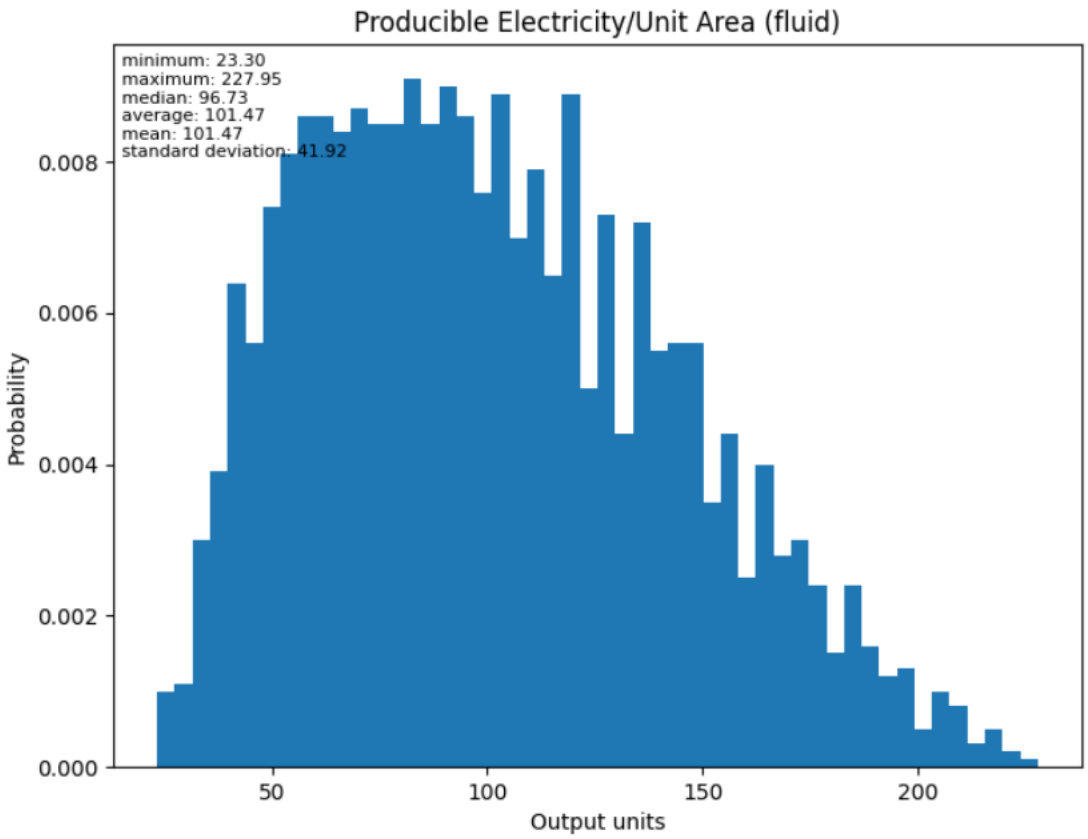

Figure 6. An example HIP-RA MC simulation for 2,500 iterations for the Interior Region, Basement Reservoir (Wisian et al., 2024). Units are in MW.

GEOPHIRES approach

We use the GEOPHIRES tool for more detailed techno-economics (Beckers, 2019). GEOPHIRES tool incorporates up to 150 input variables, yielding valuable and relatively accurate results within a +/- 15% margin. GEOPHIRES offers a comprehensive economic analysis, including a sales price model, allowing it to calculate critical project economic metrics, such as

Net Present Value (NPV), Internal Rate of Return (IRR), and Value Investment Ratio (VIR) – all vital for investors. Additionally, GEOPHIRES can compute the Levelized Cost of Electricity (LCOE), as well as its variations like LCOH (Levelized Cost of Heating), LCOC (Levelized Cost of Cooling), and LCOCS (Levelized Cost of Carbon Sequestration). Although the LCOE is the standard metric for evaluating energy-related investments, it is not entirely fair for renewable resources such as geothermal energy.

LCOE is not an entirely fair metric for evaluating various renewable energy resources, for example, geothermal energy, but is the standard in economic analyses. For example, when comparing renewable energy resources, LCOE does not account for periods of low wind and solar production on a given day. This becomes more significant when electricity grid demand remains high during these periods, leading to price spikes as demand surpasses supply and resulting in the use of higher-cost generation capacity to maintain service.

An important concept in this context is the "capacity factor," which refers to plant "up-time" or "in-commission rates." Electricity consumers require power at specific times, not just when generation resources are available (e.g., during sunny weather for solar panels or windy conditions for wind turbines). Geothermal plants exhibit a very high capacity factor. Their reliability and ability to provide 24/7 baseload energy significantly enhance their economic viability compared to what a single metric, such as LCOE might suggest.

RESULTS AND DISCUSSIONS

Descriptive gravity data interpretation

Bouguer gravity anomaly maps are essential tools for investigating subsurface structures and potential mineralization bodies. These maps come in different resolutions; each facilitates a unique purpose in geological studies. As mentioned previously, we found that the gravity data from the industry had a better resolution than publicly available data; therefore, we used this data for subsurface interpretations, including forward and inverse modeling. Based on our gravity-data interpretations, there are several basins and sub-basins present in the study area, including Presidio Bolson, Redford Bolson, Valentine Basin, and Marfa Basin.

Kucks and Robert (1999) prepared Bouguer data grid map with a grid interval of 4 km for the conterminous United States. Later, Bankey (2006) created a complete-Bouguer gravity anomaly grid map with 2 km grid spacing using approximately 76,000 gravity observations from within and around the state of Texas. This data were obtained from the gravity database maintained by the National Geophysical Data Center (Hittleman et al., 1994) and augmented with data from the USGS as well as several university theses and dissertations. Using the Texas gravity database from Bankey (2006), we prepared a Bouguer gravity anomaly map for the Presidio area (**Figure 7**). The high-resolution Bouguer gravity anomaly map was created with 500 m grid spacing using the data from Getech (**Figure 8**). Comparing the high-resolution Bouguer anomaly map to the coarse-scale gravity anomaly map, localized features corresponding to the Sierra Vieja Mountains, Valentine and Marfa basins, as well as Presidio Bolson are more distinctly highlighted in the high-resolution Bouguer anomaly map **(Figure 8)**. Interestingly, in the Big Bend region, both maps exhibit similar Bouguer gravity anomaly patterns, suggesting that the shallow anomaly feature extended to deeper depths (**Figures 7 and 8**). In contrast, a high-resolution anomaly map emphasizes localized subsurface geological characteristics, i.e., it distinctly exhibits basin geometries and structures (**Figure 8**).

The Presidio Bolson, located on the west side of the Chinati Mountains, is characterized by pronounced low Bouguer anomalies. Similarly, the Valentine Basin also displays significantly low Bouguer anomalies, oriented north-south (**Figure 8**). The basin is affected by faults. The Sierra Vieja Mountains, situated on the western side of the Valentine Basin, are marked by relatively high anomalies with NW-SE strike. Unlike the Sierra Vieja Mountains, the Chinati Mountains exhibit low-to-moderate gravity anomalies. Low gravity anomalies are likely related to the Marfa Basin sediments, which were emplaced in the Chinati Mountains during the Laramide deformation, Basin and Range faulting, and Tertiary volcanic activity (Rix, 1953; Kopp, 1977; Mraz and Keller, 1980; Keller et al., 1981). In the central region, moderate gravity anomalies are prevalent and associated with the Marfa Basin (**Figure 8**). A few relatively high Bouguer anomalies with irregular shapes fall in the central area (around Big Bend area) may be linked to the Tertiary intrusions. In the northeastern corner of the study area, the Crenshaw Mountains are associated with high anomalies trending north-south. Broad and extensive high Bouguer anomalies are observed over the Bofecillsos Mountains northeast of Presidio (**Figure 8**). This region comprises a diverse assemblage of volcanic and plutonic rocks (Barker, 1977; Miggins et al., 2008). These rocks are possibly responsible for the pervasive high Bouguer anomalies in the Bofecillsos Mountains.

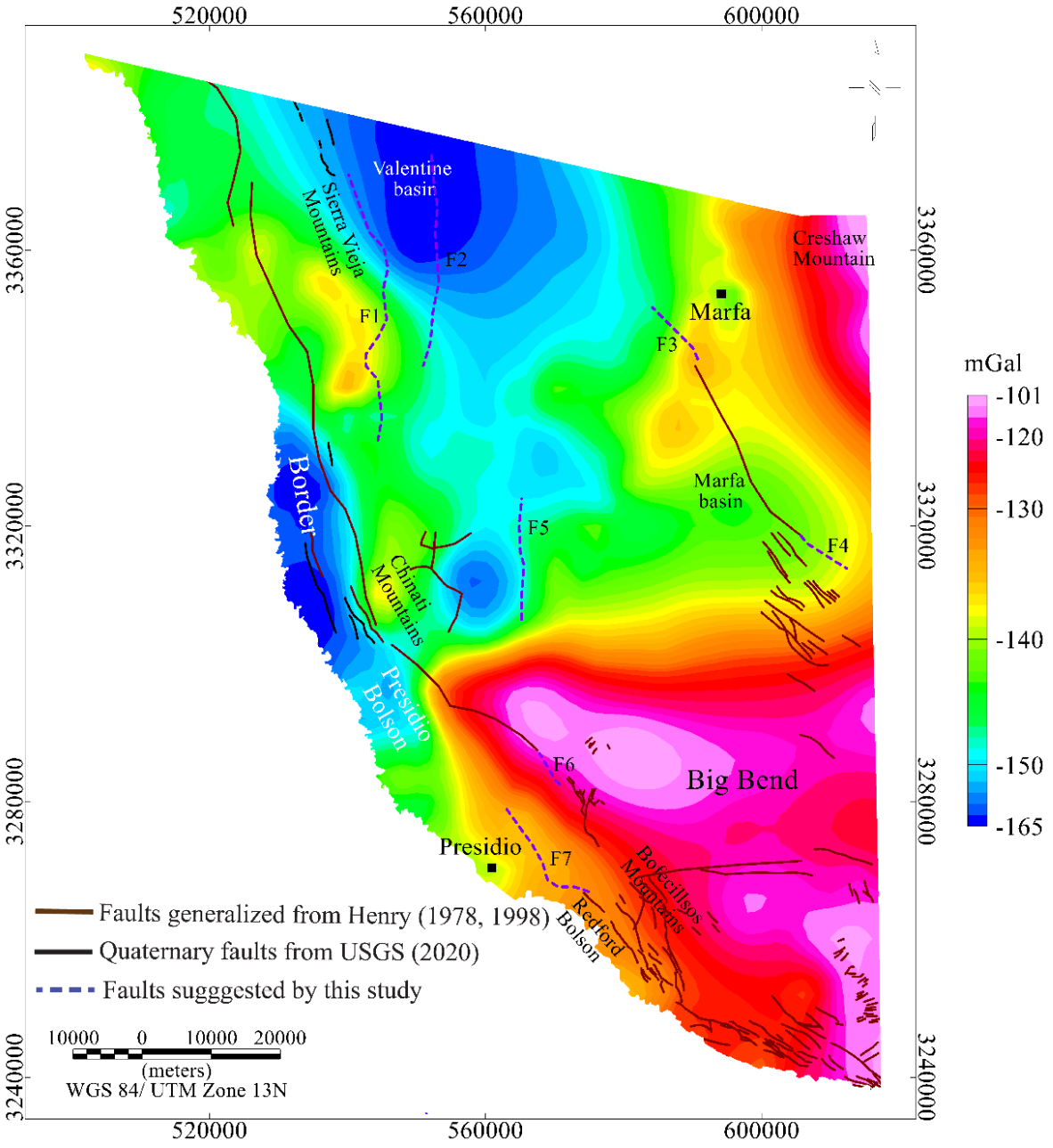

Figure 7: Bouguer gravity anomaly maps sourced from United States Geological Survey (data from Bankey, 2006)

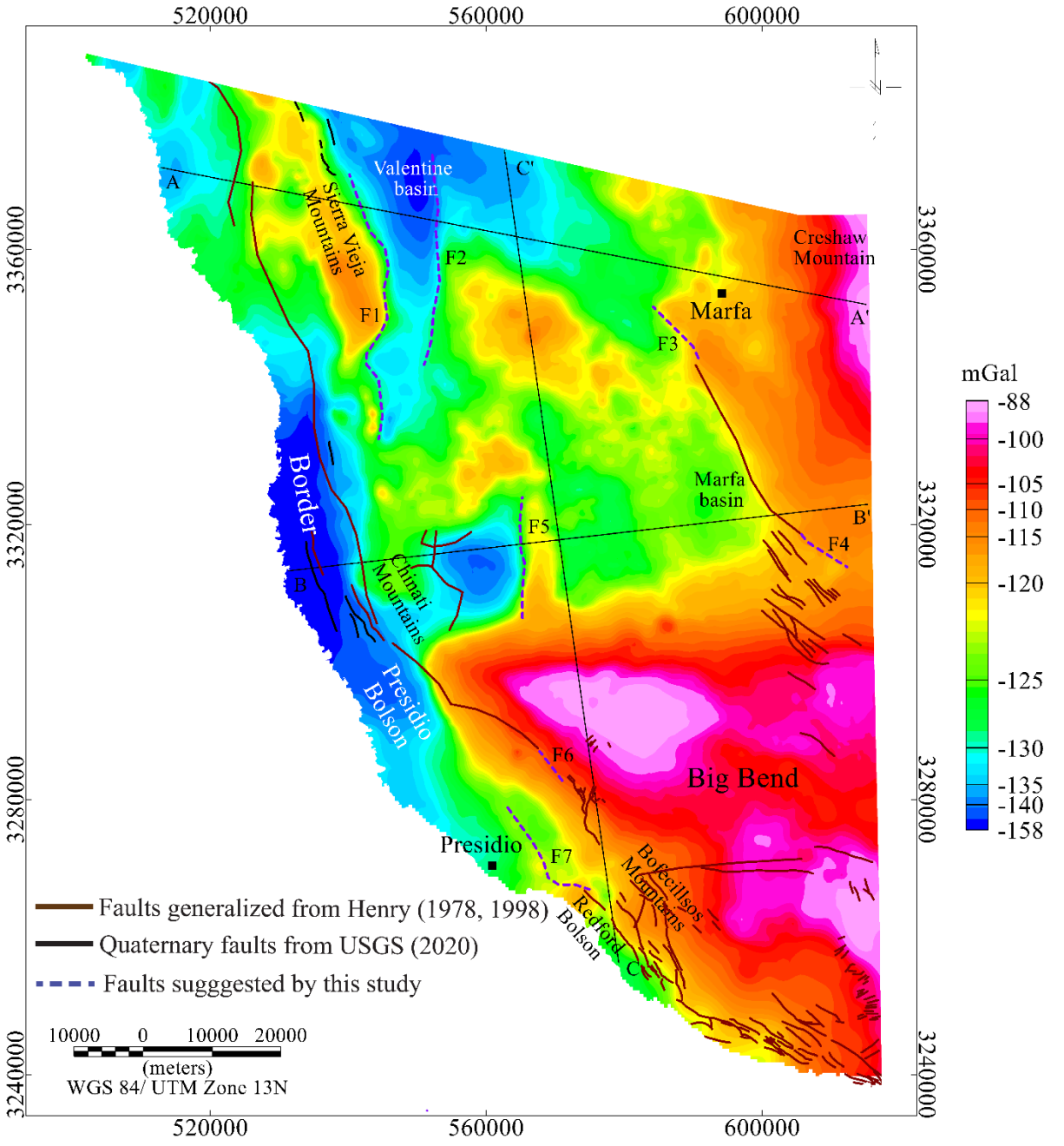

Figure 8: High-resolution Bouguer gravity anomaly maps sourced from Getech Group Plc. Profiles AA' to CC' lines in **Figure 8** indicate the location along which 2D forward Bouguer gravity models were generated, which are shown in Figures 11 to 13.

Total horizontal derivative and tilt angle derivative maps of Bouguer gravity anomalies

The application of total horizontal derivative (THD) and tilt derivative (TDR) filters to high-resolution Bouguer gravity anomalies is highly effective in identifying the edges of the geological features, such as faults or boundaries between the various geological domains (Roest et al., 1992; Blakely, 1996; Miller and Singh, 1994; Salem et al., 2007). Peaks observed in the THD map represent the sharp boundaries and edges corresponding to high-density contrast (Roest et al., 1992; Blakely, 1996) (**Figure 9a**). The TDR tool is particularly useful for detecting weaker anomalies and facilitating a more balanced view across varying depths (Miller and Singh, 1994). The zero-degree contours in the TDR map delineate the edges of the geological structures (**Figure 9b**).

In this study, we employed THD and TDR techniques to Bouguer anomalies from Presidio to detect sharp edges or boundaries of geological features. The results revealed several new faults and extensions of previously interpreted faults (Brown, 1963; Henry 1979a, b; Henry, 1998) (**Figure 9**). Specifically, new faults include F1, F2, F3, F4, F5 in the Interior region, F6 over the Bofecillsos Mountains and F7 in the Redford Bolson (Figure 9). The newly identified F1 and F2 faults, which coincide with western and eastern borders of the Valentine Basin, respectively, might represent the edges of the graben structure, as suggested earlier by Covert (1976), who proposed that the basin is likely a Cenozoic graben. According to earlier studies (Rix, 1953; Kopp, 1977; Mraz and Keller, 1980; Keller et al., 1981), Chinati Mountains have experienced Laramide deformation, Basin and Range faulting, and Tertiary volcanic activity. Therefore, the proposed faults, F5 in the Chinati Mountains may be associated with concealed Basin and Range fault. Additionally, extensions of previously known faults were noticed, such as F3 and F4 in the Interior region and F6 in the Bofecillsos Mountains (**Figure 9**).

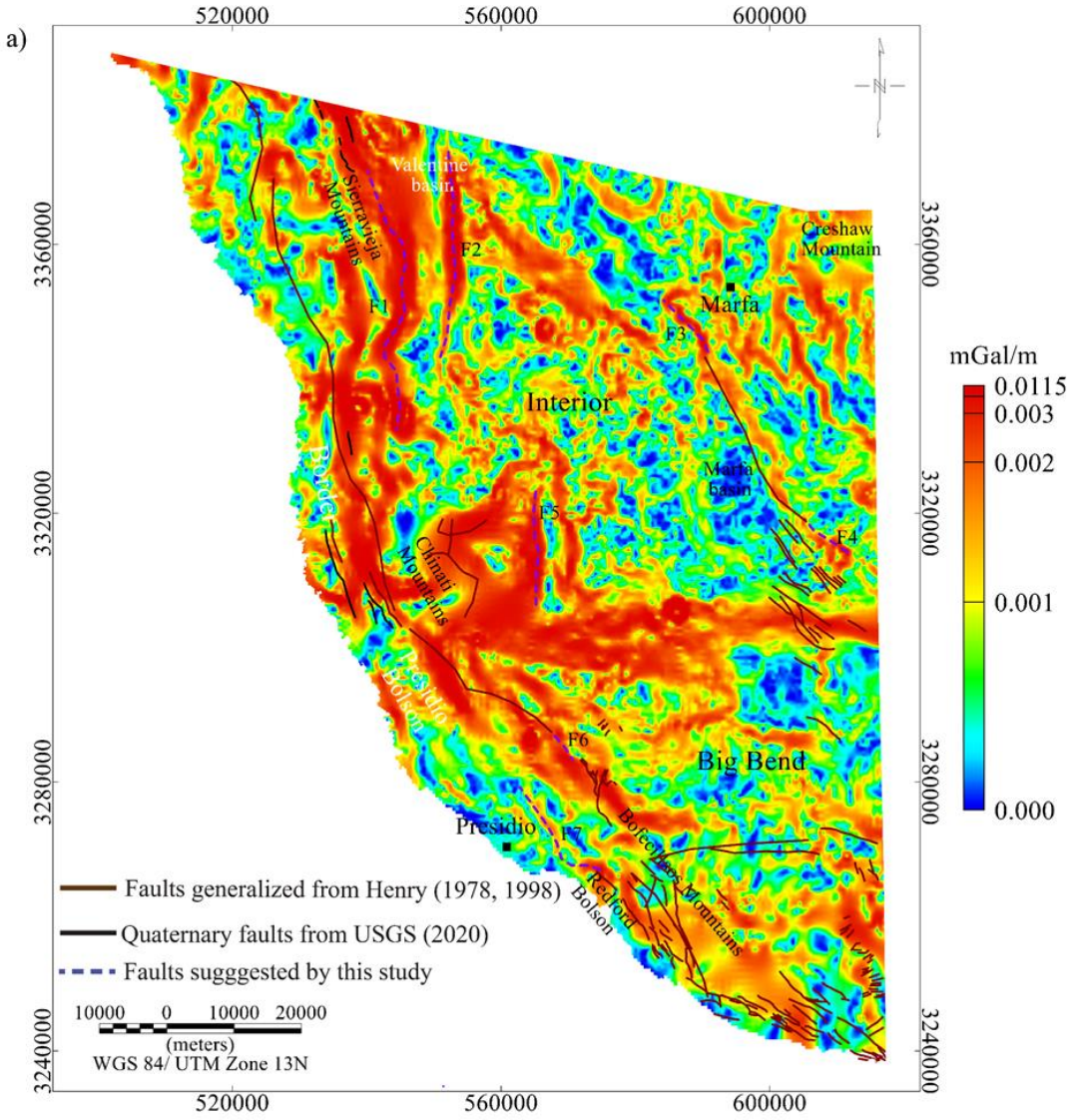
a)
520000
560000
600000
3360000
3320000
3280000
3240000
Valentine basin
Sierravieja Mountains
F1
F2
Creshaw Mountain
Marfa
F3
Interior
Marfa basin
F4
F5
Chinati Mountains
Presidio Bolson
F6
Big Bend
Presidio
F7
Bofecillos Mountains
Redford Bolson
mGal/m
0.0115
0.003
0.002
0.001
0.000
Faults generalized from Henry (1978, 1998)
Quaternary faults from USGS (2020)
Faults sugggested by this study
10000 0 10000 20000
(meters)
WGS 84/ UTM Zone 13N

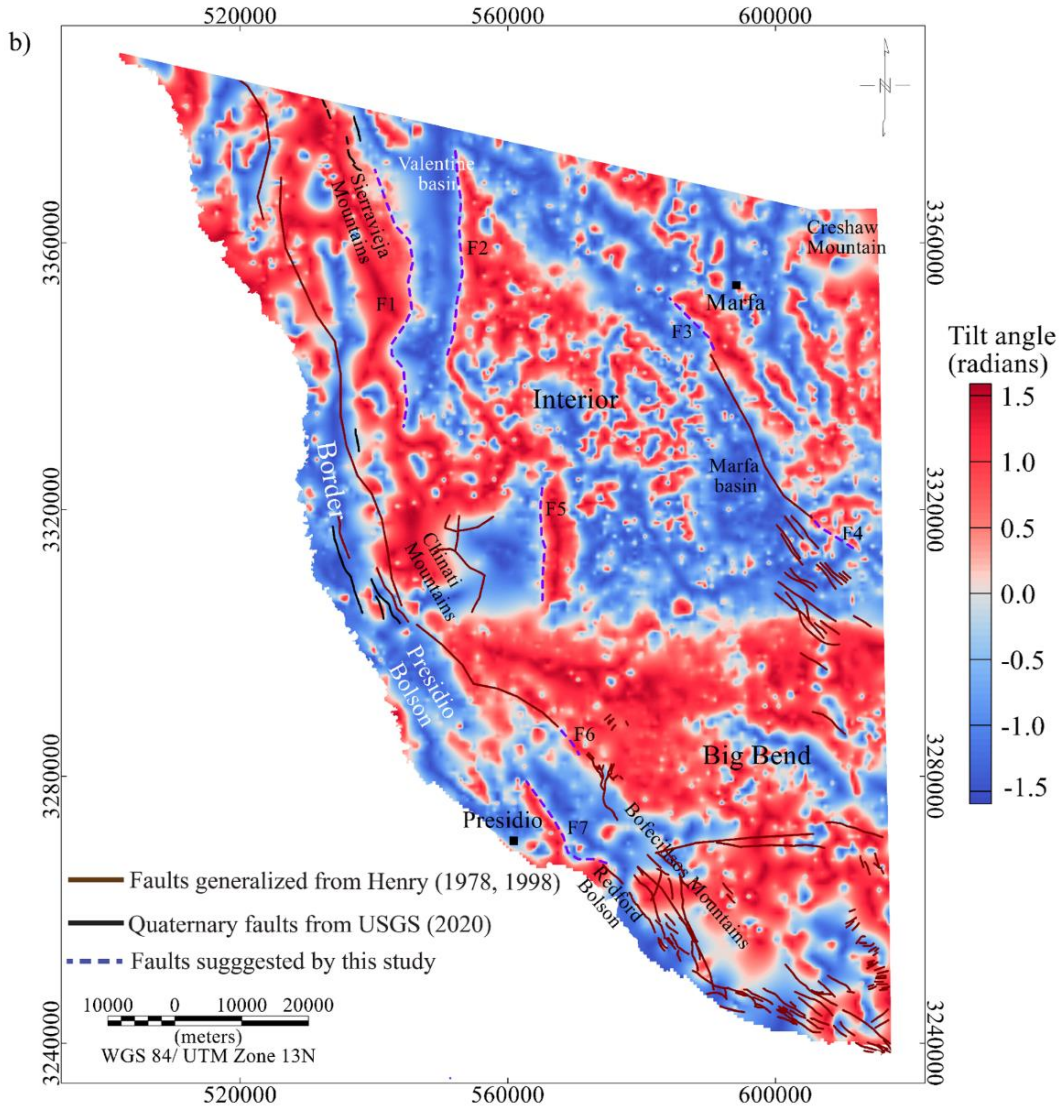

Figure 9. a) Total horizontal derivative, b) Tilt derivative maps of Bouguer anomalies from high-resolution gravity data, respectively.

Estimates of Precambrian basement depth from 3D gravity inversion

We conducted a 3D gravity inversion of the high-resolution gravity data to estimate the Precambrian basement depths in the Presidio area. The resulting basement depth map indicates that the basement depth ranges from 0 (surface) to ~6 km, as shown in **Figure 10**. The Presidio Bolson is characterized by a deep basement depth, predominantly around 4 to 6 km (**Figure 10**). In the Bofecillsos Mountains (in the Big Bend area), on the other hand, it is noticed that the central portion of this area has no sediment cover. However, the periphery of this area attained shallow basement depths, ranging between 0.5 and 2 km. The Marfa Basin displays a variation in basement depth from shallow to deeper basement depths, spanning 0.5 to 4 km (**Figure 10**). The basement depths in the Marfa Basin gradually decrease from the central portion towards the northeast, reaching depths of 0.5-2 km (**Figure 10**). The Valentine Basin is associated with notably deeper basement depths of approximately 4 to 5 km. Similar deeper basement depths (~4-6 km) are also found over the Chinati Mountains **(Figure 10**). Compared to the existing borehole results (BH-1 and BH-2), the obtained basement depth is closely matched with BH-1 basement depth, but it shows more deviation (~ 1 km) at BH-2. One of the possible reasons for this deviation could be a significant lateral density variation within this study area that is beyond the resolution of the available geophysical data.

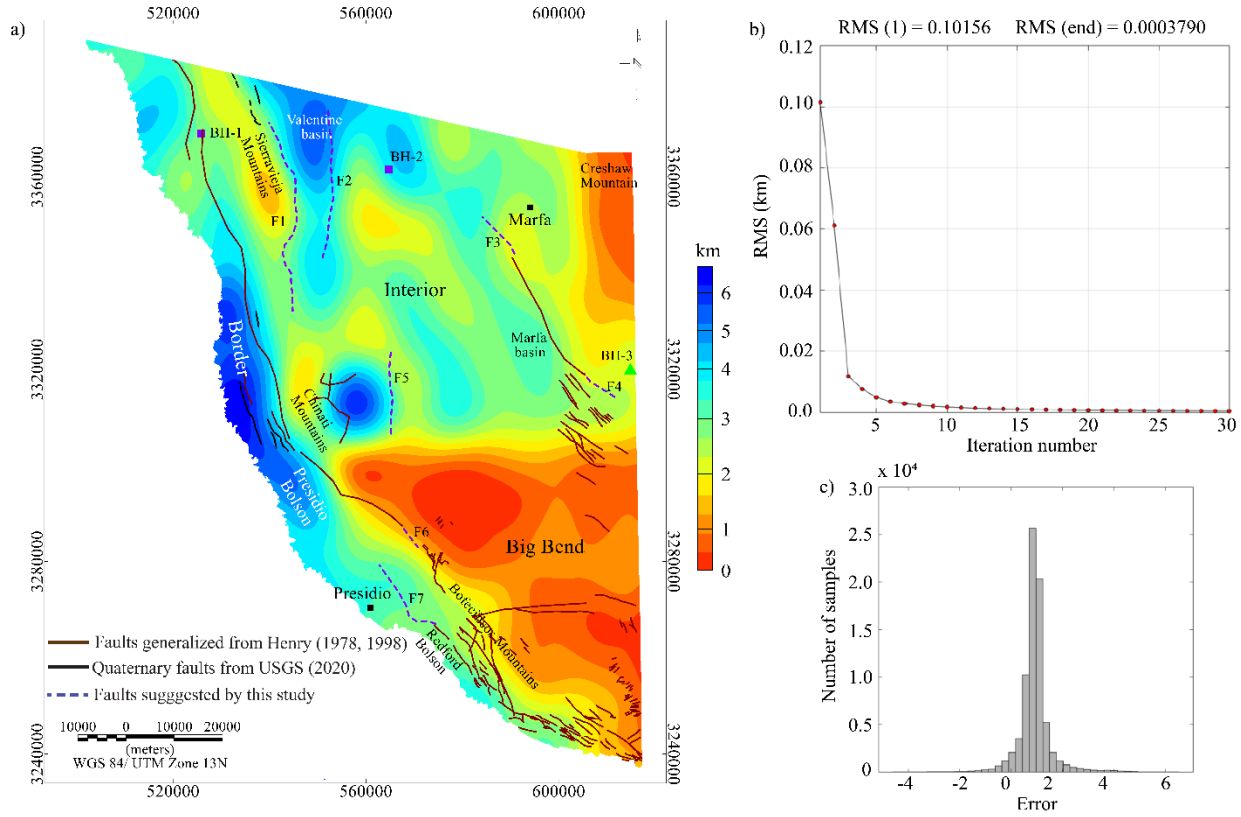

Figure 10. a) Precambrian basement top depth map obtained from 3-D inversion of Bouguer anomalies from high-resolution gravity data. b) Root mean square (RMS) error plot of the Bouguer anomalies. c) Histogram plot of the error.

Basin cross-sections from 2D forward modeling of Bouguer gravity anomaly data

To better understand the basin structures, 2D forward gravity modeling was conducted along three profiles (profile-AA' to CC') (see Figure 8 for the profile location). The profile AA' extended across Presidio Bolson, Sierra Vieja Mountains, Valentine Basin, Marfa Basin, and Crenshaw Mountains. While profile-BB' crossed the Presidio Bolson, Chinati Mountains, and Marfa Basin. Both profiles AA' and BB' fall in the approximately east-west direction. The third profile lies north to south and crosses the Redford Bolson, Bofecillos Mountains, Marfa Basin, and Valentine Basin. Based on previous geologic (Brown, 1963; Kopp, 1977; Henry 1979a, b; Henry, 1998) and geophysical (Mraz and Keller, 1980; Keller et al., 1981) studies and borehole data used in this study, we considered following geological units in models: Bolson fill (1,900 kg/m^3), Tertiary volcanic (2,000 kg/m^3), Mesozoic sediments (2,300 kg/m^3), Paleozoic sediments (2600 kg/m^3), Precambrian basement (2,700 kg/m^3), and Intrusive (2,800-3,000 kg/m^3) (**Table 1**). The initial basement geometry was constrained based on borehole data and estimated basement depth from 3D gravity inversion. After constructing the 2D initial basement models, Talwani et al. (1959) algorithm was utilized for computing the forward response of the Bouguer anomalies.

The results of gravity models along three profiles (AA' to CC') reveal complex basin structures, including faults, igneous intrusive, the basement variations ranging from 2 to 5 km beneath the Presidio County region (Figures 11-13). The significant deep basement depths (4-5 km) are observed below the Presidio Bolson, Valentine Basin, and eastern portion of the Marfa Basin (**Figures 11-13**). There are some areas near the border region, where the Precambrian basement is shallow 2.5 km (~8,000-9,000 ft in depth), which is also confirmed by borehole data and associated mud logs. These areas might also receive elevated heat flow contributions from radiogenic heat production as well as a thinner crust due to basin and range extension. Chinati Hot

Springs is on the east side of Presidio Bolson. Unlike Presidio Bolson, the Redford Bolson is characterized by a shallow basement depth of approximately 2.4 km. The Bofecillsos and Sierra Vieja Mountains exhibit shallow basement depth of 2-2.2 km, and 2.5-3.0 km, respectively (**Figures 11-13**). Comparatively, Chinati and Creshaw Mountains display relatively deeper basement depths of approximately 3.4-4 km (**Figures 11-13**). The Marfa Basin exhibits relatively shallow basement at most places but can be as deep as 5 km at places (verified from borehole data).

Table 1. Considered density values in 2D forward gravity models

Formation	**Density (kg/m^3)**
Bolson fill	1,900
Tertiary volcanics	2,000
Mesozoic sediments	2,300
Paleozoic sediments	2,600
Precambrian basement rock	2,700
Intrusives	2,800-3,000

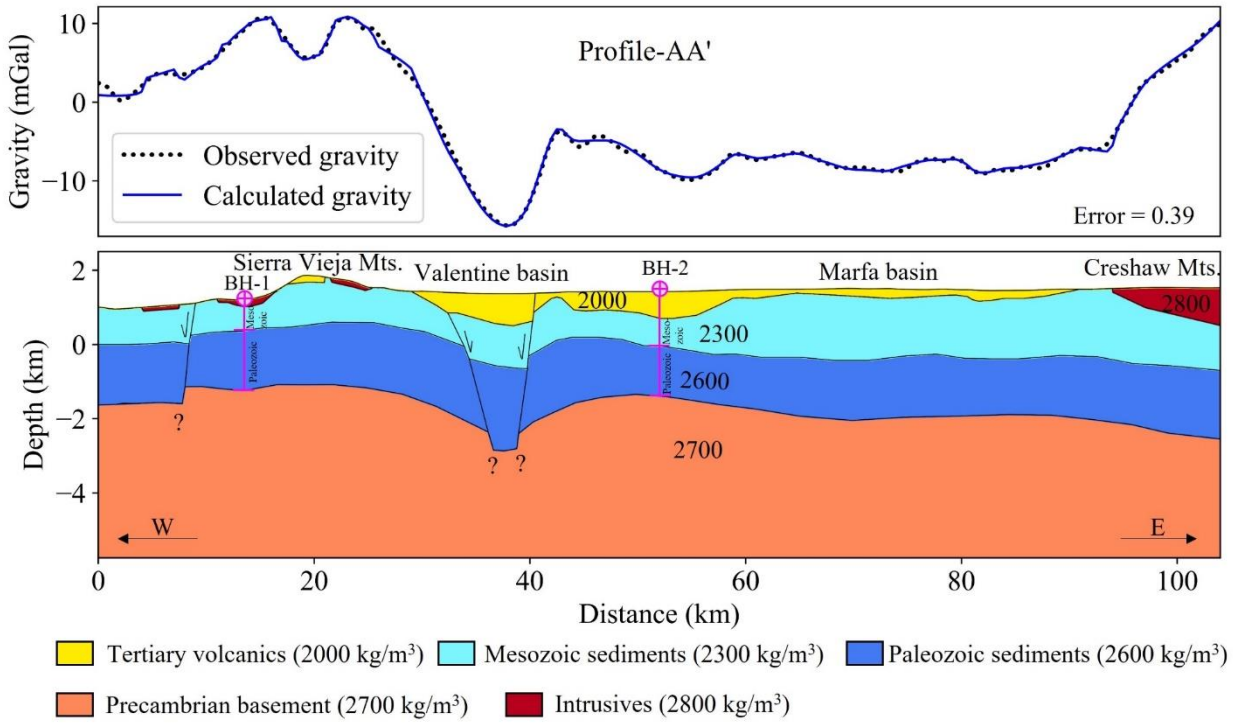

Figure 11. The basin cross-section model along profile AA' was obtained from 2D forward gravity modeling constrained with borehole data and 3D basement depth derived from 3D gravity inversion (see **Figure 8** for profile location). Two deep boreholes (BH-1 and BH-2) were used to constrain the inversion results.

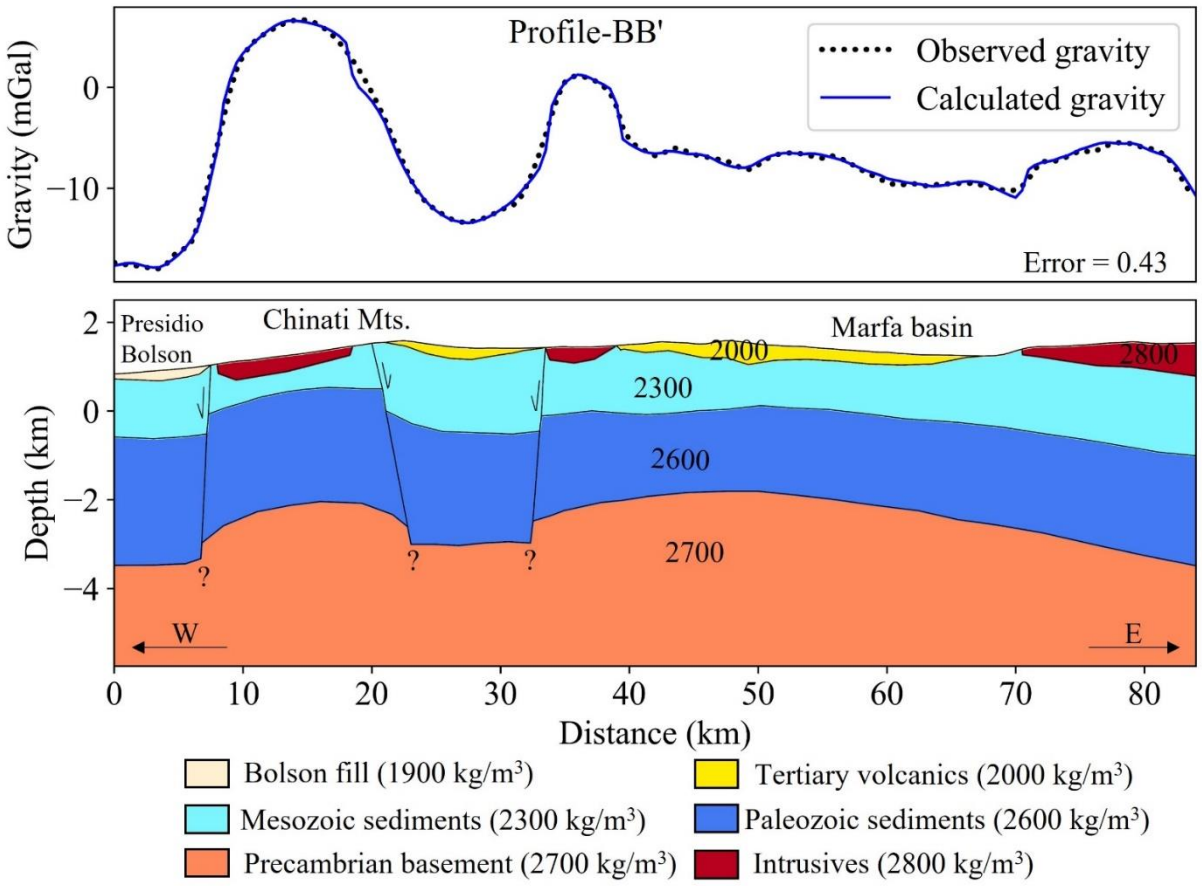

Figure 12. The basin cross-section model along profile BB' was obtained from 2D forward gravity modeling constrained with borehole data and 3D basement depth derived from 3D gravity inversion (see Figure 8 for profile location).

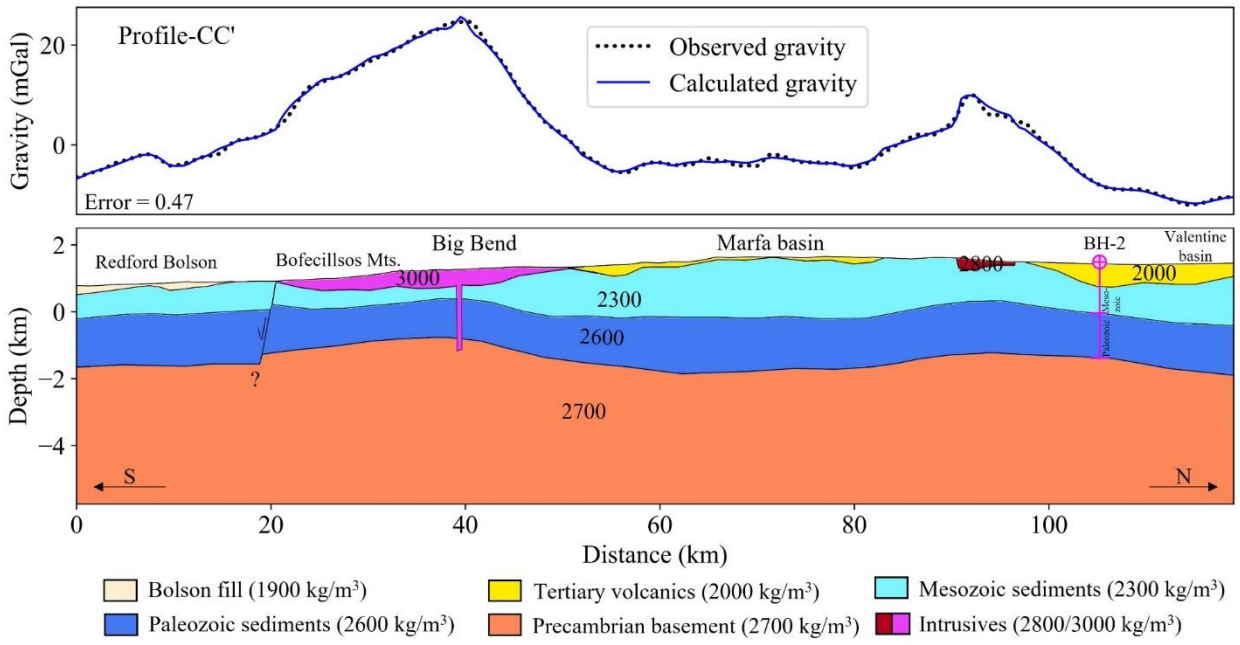

Figure 13. The basin cross-section model along profile CC' was obtained from 2D forward gravity modeling constrained with borehole data and 3D basement depth derived from 3D gravity inversion (see Figure 8 for profile location).

Based on our gravity inversion results, the basement structure varies laterally, affected by faults. This is also confirmed by the tilt derivative maps. A combined analysis of tilt derivative and inversion methods indicates several basin-bounding faults. A large portion of the Marfa Basin is shallower than both Presidio Bolson and Valentine Basin.

Thermal Regime

Temperatures in the Interior Region

Corrected BHT (after Harrison's correction) for the Interior Region are illustrated in **Figure 14**, showing a maximum of 160°C at a depth of 4,870 meters. While there is some moderate

data scatter, it reveals a near-linear trend of increasing temperatures with depth. We constructed a simple temperature model using rock type and associated thermal conductivity values, which are presented in **Table 2.**

Table 2. Thermal conductivity of rocks at various depth intervals in the study area

Depth (m)	**Thermal Conductivity (k) (W/m-K)**
0-1,457	3.63
1,457-6,001	3.0
6,001-7,850	3.3

We set the ambient temperature to 15°C. Assuming a constant heat flow, we extrapolated the modeled temperatures downward sequentially using the standard heat flow equation:

$$\Delta T=(\Delta D*HF)/k$$

Where ΔT is the change in temperature across the layer, ΔD is the thickness of the layer, k is the thermal conductivity of the layer, and HF is the crustal heat flow, assumed to be a constant. In this case, we assumed no radiogenic heat production. **Figure 14** shows the modeled temperature-depth plot for the Interior region. The changes in overall thermal conductivity for the generalized rock types in the subsurface are relatively small, ranging from 3.0 to 3.63 W/m·K, which shows up as slight changes in the geothermal gradient values in the dark green line in **Figure 14**.

In this model, the heat flow (HF) was adjusted until the modeled temperatures best fitted the observed BHT data. For the Interior Region, the estimated HF is 95 mW/m². Although this

figure is lower than that of the Border Region, it remains above the world average continental HF of 71 mW/m² (Davies, 2010), which makes this target promising. In contrast, the overall heat flow range in the Basin and Range province typically spans 60-100 mW/m² (Blackwell et al., 2011).

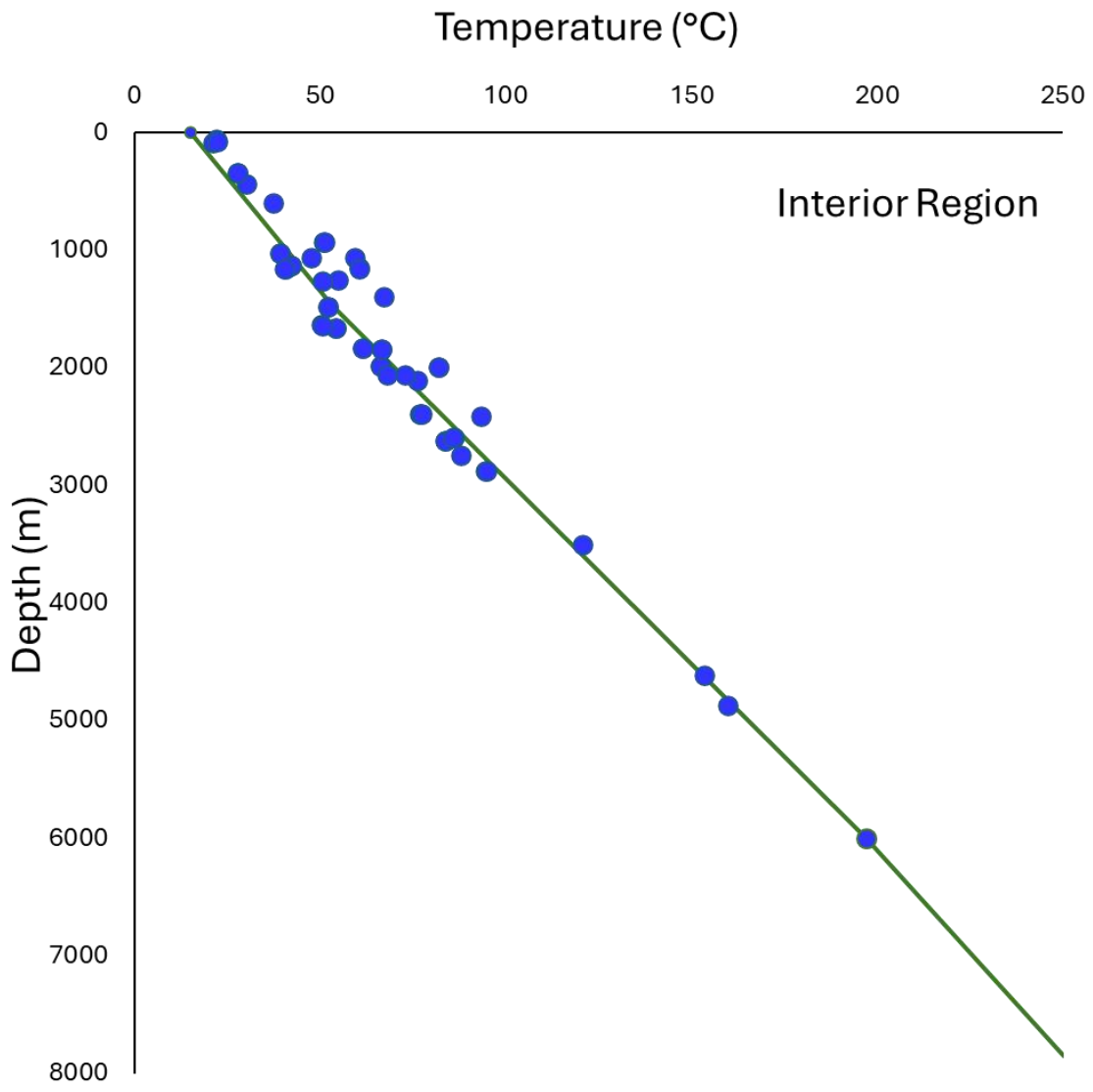

Figure 14. Temperature-depth plot for the Interior region, with BHTs in blue and modeled temperature curve in dark green.

Temperatures in the Border Region

The Border Region exhibits significantly higher temperatures than the adjacent Interior Region (**Figure 15**). The estimated heat flow (HF) in the Border Region is 155 mW/m², which is at the upper end of the Basin and Range heat flow range. In some areas of the Border Region, the Precambrian basement depth is relatively shallow (~2.5 km) and presents a suitable target. However, proper basement characterization needs to be done, in terms of rock composition, petrophysics, geomechanics, and faults.

The temperatures in shallow formations (with depths less than 300 meters/~1,000 ft) in the Border Region (**Figure 15**) consistently exceed the predictions made by our model. Several factors may account for this discrepancy: 1) random noise, 2) temperature measurements taken predominantly during the warmer months, 3) the presence of a shallow thermal anomaly, or 4) upflow of groundwater from greater depths. Localized disturbances in temperature due to water upflow seem to be the most plausible explanation, which requires further investigation. Although the hot, shallow formations are not suitable for power generation, they offer options for direct-use, warranting additional exploration.

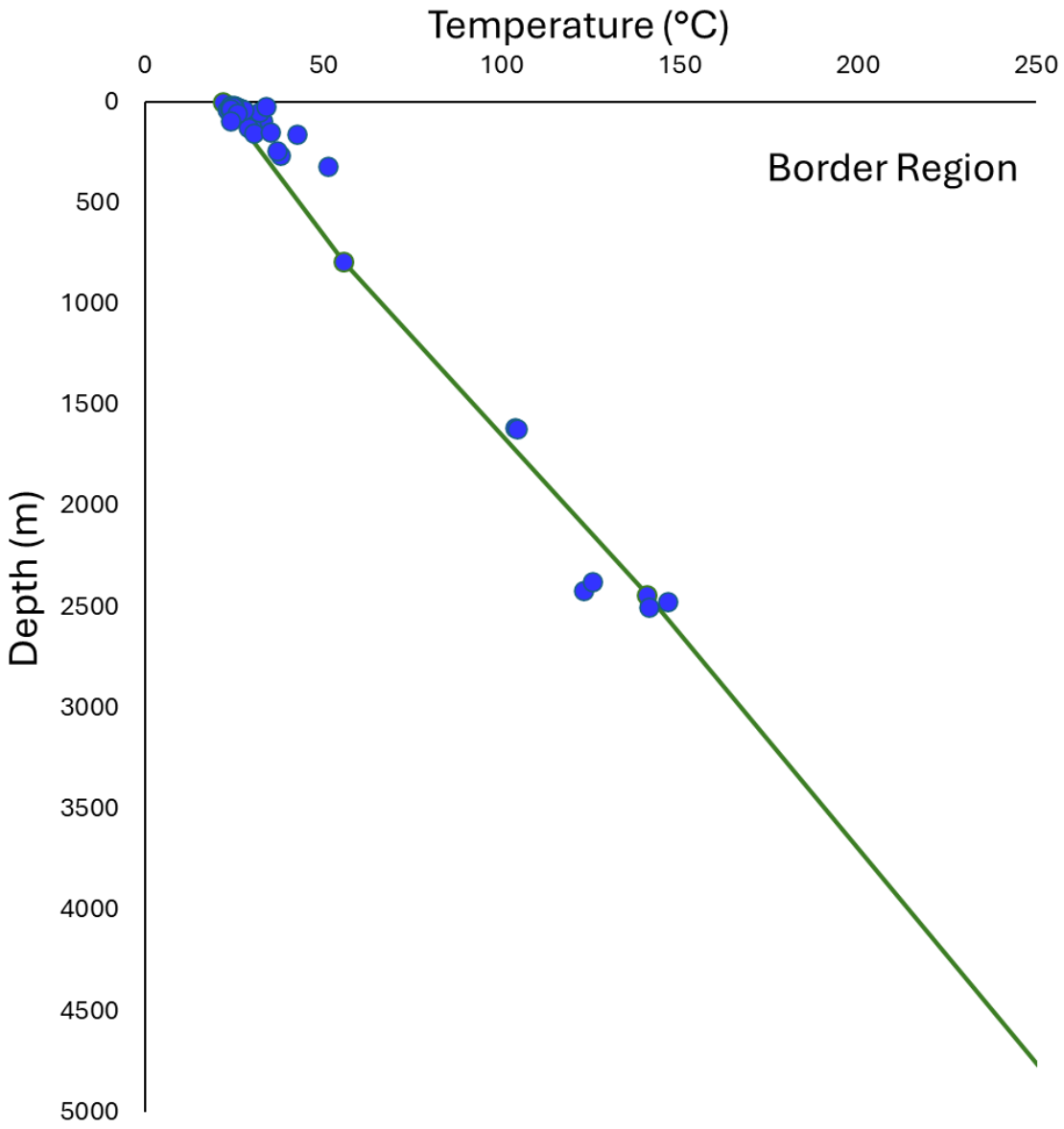

Figure 15. Temperature-depth plot for the Border region, with BHTs in blue and modeled temperature curve in dark green. Note the cluster of temperatures at the shallow depth (<300 m/~1,000 ft), which were removed for geothermal gradient estimates in the deep subsurface.

Formation lithology and reservoir properties

Based on our interpretation of the limited well logs and core data, we constructed a simplified litho-stratigraphic column representing the overall study area (**Figure 4**). Due to the scarcity of subsurface information in our study area, we utilized outcrop data where appropriate and developed generalized models of the subsurface at a regional scale. The simplified stratigraphic column depicts the geological ages ('era') and representative lithology in the subsurface. The stratigraphic column is primarily composed of three rock sequences: Precambrian basement (mixture of arkosic sandstone, granite, rhyolite, quartzite, etc.), Paleozoic-Mesozoic carbonates mixed with shale and sandstone, and Tertiary volcanics, volcaniclastics, and intrusives. Carbonate rocks are dominant during the Paleozoic-Mesozoic era (for example, Ellenburger or equivalent El Paso Group). Due to the limited number of boreholes and core samples, multiple basins, and lack of lithologic continuity, we decided not to subdivide these carbonates in the deep subsurface into distinct formations or correlate them across the basins in the study area. We recommend a more detailed, site-specific geologic and geophysical analysis before commencing any development project.

Reservoir properties from well log analysis

We also analyzed available petrophysical logs and mud logs from 14 wells and relevant literature to identify general rock types and estimate their depth of occurrence, porosity, density, and thermal conductivity (**Table 3)**. Carbonate rocks exhibit slightly higher porosity, reaching up to 9 p.u. (%). Tertiary rocks show a wide range of porosity estimates due to their intercalation with volcanic, volcaniclastic, and intrusive rocks that have different pore characteristics. For formations lacking laboratory measurements of thermal conductivity, we relied on analogous formations.

Fracture studies

We identified two distinct groups of fractures in the Ellenburger Group (equivalent to El Paso Group) in the Gulf Mitchell Bros. State No. 1 core. The oldest fractures are the most numerous; have irregular shapes, sediment or mineral fills, show wide range of aperture size (sub mm to multi-mm), and no preferred orientation. This group of fractures have been attributed by previous workers to karst-related brecciation associated with the collapse of Lower Ordovician paleocave systems (Kerans, 1990; Loucks, 1999; Gale and Gomez, 2007). Karst-related fractures are usually closely spaced with less than an inch apart and tend to be bounded by stratigraphic beddings or stylolite.

Loucks (1999) classify breccias into crackle breccia, mosaic breccia, and chaotic breccia, which are all observed in the Gulf Mitchell Bros. State No. 1 core. Crackle breccias (**Figure16a**) have thin, closely spaced fractures separating breccia clasts. Mosaic breccias (**Figure16b**) are similar to crackle breccias, but displacement between clasts is greater, and some clast rotation is evident. Chaotic breccias (Figure16c) are characterized by extensive rotation and displacement of clasts. Some interbreccia porosity is preserved, but most of it has been occluded by dolomite cement.

The youngest group of fractures are subvertical, opening-mode fractures crosscut the older karst-related fractures and saddle dolomite and are observed throughout the Ellenburger section in the Gulf Mitchell Bros. State No. 1. These fractures are thought to have a tectonic origin and were formed during the late stages or after the Pennsylvanian Ouachita orogeny (e.g., Loucks and Anderson, 1985; Kerans, 1989; Kerans, 1990). Tectonic fractures are usually narrow (<0.5 mm aperture) and may or may not show hints of mineral cement on the fracture surface (**Figures 17a, 17b, 17c**). The core usually breaks apart along these fractures, however, the existence of cement

on the fracture surface indicates that the fractures were formed and present in the subsurface. Tectonic fractures are generally spaced at >1-inch scale, also longer and more through going (> 1ft in length), cutting across earlier fractures, stylolite, and stratigraphic beddings. Although fracture orientation cannot be obtained from our core, Gale and Gomez (2007) reported this group of fractures generally show northeast-southwest and northwest-southeast strikes, measured in some sidewall cores from two wells in Regan County from the Permian Basin of west Texas.

The most common porosity type observed in the Ellenburger section from the Gulf Mitchell Bros. State No. 1 core occurs in (1) brecciated dolostones within paleokarst collapse zones (**Figure 15**), (2) late tectonically generated fracture porosity (**Figures 16a, 16b**), and (3) vuggy and intercrystalline porosity in dolomitized microbialites and along zones of preferential permeability (**Figure 16e, 16f, 16g**).

Matrix porosity in cave-sediment fill, in host wall rocks, and in breccia clasts are very low. Thus, higher porosity zones segmented by impermeable cave-infill sediments may result in vertical reservoir compartmentalization (Kerans, 1990). Cavernous porosity was reported to be a key component in the Ellenburger paleocave pore networks (e.g. Loucks, 1999), which is indescribable in our core. However, the fact that the core is broken into smaller pieces that are hard to put back together may be indicative of the existence of cavernous porosity in the subsurface.

Multiple-episode cave system subsides and collapses can result in the enhanced interconnection of breccias, vugs, and fracture systems (Loucks, 1999). However, the porosity associated with those features is not necessarily well connected in the subsurface. A better connectivity of the porosity may be achieved by reservoir stimulation for geothermal development purposes.

In addition to the two distinct groups of fractures, we observed porosity and carbonate cement developed along subvertical, tectonic-origin stylolites are an important component of this cored Ellenburger section. Carbonate minerals fill along the tectonic stylolites implied an episode of porosity creation after emplacement of these stylolites (**Figure 17d**). We also observe fracture terminates against the stylolite at high angle (**Fig 17d**) indicating the stylolites may act as mechanical interfaces in the rock. While most of that porosity has been filled by cement and is not conductive of fluid flow present day, the stylolite may act as planes of weakness and prone to be reactivated during geothermal reservoir stimulation.

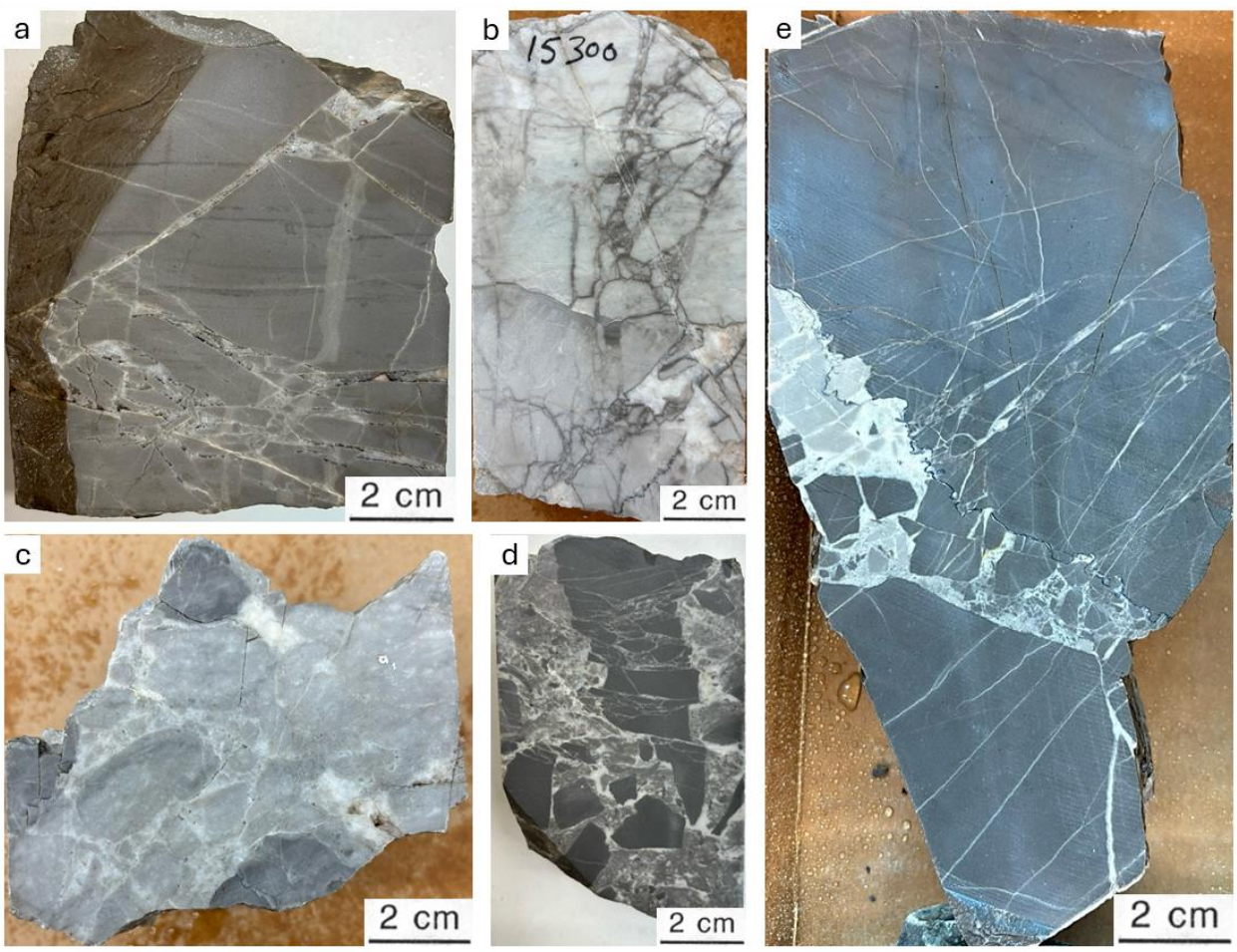

Figure 16. Examples of Ellenburger paleokarst breccias, Gulf Mitchell Bros. State No. 1, Presidio County, SW Texas. a). Crackle breccia and persistent interbreccia fracture porosity, pervasive network of fractures lined by saddle dolomite, 15,809 ft (~4,819 m). b). Mosaic breccia, interbreccia fracture porosity largely occluded by dolomite cement, 15,300 ft (~4,663 m). c). Clast-supported chaotic breccia showing mixed clast types with persistent interbreccia porosity, 15,453 ft (~4,710 m). d). Chaotic breccia with clasts that show crackle brecciation from mechanical compaction, interbreccia fracture porosity occluded by dolomite cement, 15,598 ft (4,754 ft). e). Crackle breccia with belt of chaotic breccia infill and pervasive dolomite cement, 15,622 ft (~4,762 m).

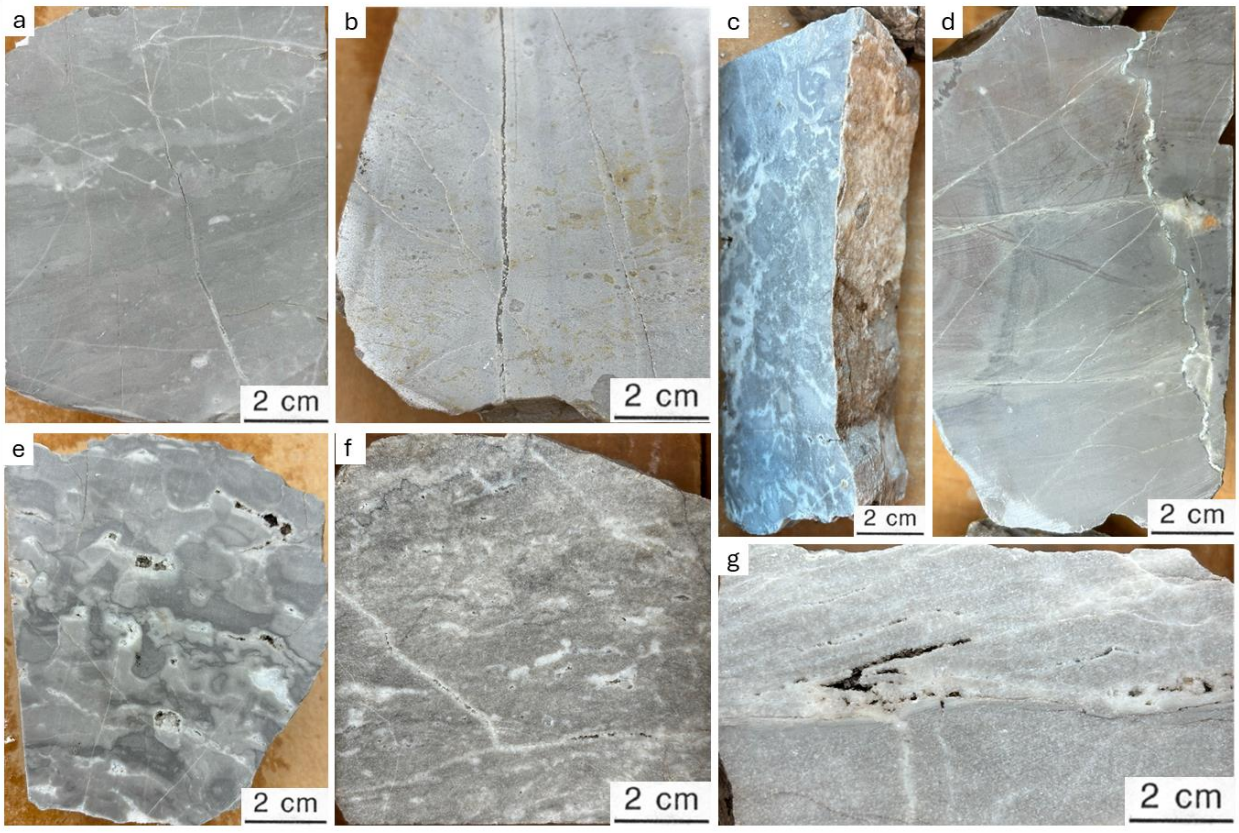

Figure 17. Core photograph of tectonic fracture porosity and porosity in microbialites. a). Partly open tectonic fractures show persistent porosity at wider part of the fracture (>0.3mm) and tend to

be completely sealed when aperture is smaller than 0.3mm towards fracture tip, 15,271 ft (~4,655 m). b). Partly open tectonic fracture (~1 mm aperture) with pillars of cement minerals grows on fracture surfaces and towards the void space in between, 15,277 ft (~4,656 m). c). Broken apart core exposes the surface of a tectonic fracture showing carbonate mineral cement lining, note the fracture cut across vuggy porosity in the microbialite, 15,672 ft (~4,777 m). d). Carbonate minerals along the tectonic stylolites, note some thin fracture terminates against the stylolite at high-angle, 15,899 ft (~4,846 m). e). Vuggy and intercrystalline porosity in pervasively dolomitized microbialites, 15,443 ft (~4,707 m). f). Enlarged porosity along fractures as path of preferential permeability in vuggy dolomitized microbialites, 15,983 ft (~4,872 m). g). Relict cross-stratification marked by vuggy porosity, 15,979 ft (~4,870 m).

Figure 18 provides a summary of the depositional system and the variation in fracture abundance with depth in the Gulf Mitchell Bros. State No. 1 core, specifically highlighting breccia and tectonic fractures. This builds on the facies characterization of the Ellenburger interval presented by Kerans (1990), which we have adopted and expanded. As shown in **Figure 18**, the abundance of breccia, or karst-related fractures, is represented qualitatively, illustrating variations among the three breccia types. In contrast, tectonic fracture abundance is quantified by the cumulative length of fractures per unit length of the core, measured at each observation interval. The resolution of our analysis is approximately 6 m (~20 ft). For instance, an abundance value of 0.5 (dimensionless) indicates that over a 20-ft section of core, the cumulative length of observed tectonic fractures totals 10 ft.

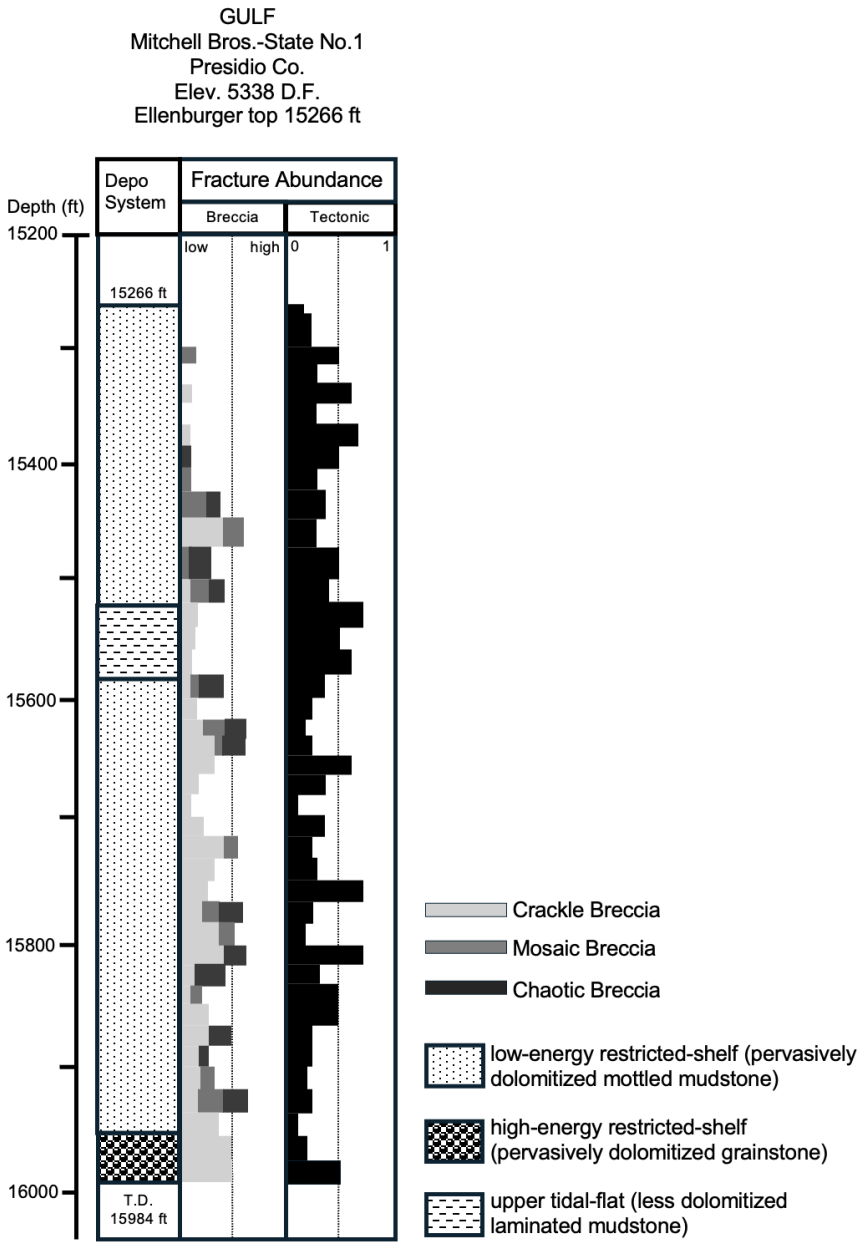

Figure 18. Depositional system and fracture abundance (including breccia and tectonic fractures) versus depth in the Gulf Mitchell Bros. State No. 1 core. Depo system and corresponding dominant facies are based on Kerans., 1990. The tectonic fracture abundance value is the total length of fractures observed in a unit length of cored interval; resolution of interpretation is ~20ft (6 m).

Table 3: Generalized rock properties in the deep subsurface in the study area, primarily based on borehole data and geophysical mapping. Underlined values indicate high uncertainties.

Reservoir	Major rock type	Mean fm. top depth	Range of fm. top depth	Mean thickness	Range of thickness	Mean porosity	Mean density	Thermal conductivity
Units		m	m	m	m	p.u.	g/cc	W/mK
Tertiary	Basalt	9	0-18	1,371	784-1,447	6	2.76	3.63
Paleozoic-Mesozoic	Carbonate	1,247	793-1,457	1,492	1,339-4,543	9	2.6	3
Precambrian	Granite	2,617	2,438-6,000	n/a	n/a	Negligible for intact rock; high for fractured rocks	2.75	3.3

Techno-economics

We used our subsurface characterization results to define geothermal exploration targets and conducted a detailed techno-economic assessment.

Regional HIP-RA Analysis

We divided the HIP-RA analysis into three geographical areas, each characterized by distinct geologic properties: Border, Interior, and Big Bend. For each zone, we conducted three analyses representing three fundamentally different reservoirs observed in the study area, referred to as “Tertiary” (the youngest, shallowest, and coolest), “Paleozoic-Mesozoic (PzMz)” (intermediate in terms of age, depth, and temperature), and “Basement” (the oldest, deepest, and hottest). In total, nine simulations were conducted (three regions multiplied by three reservoirs per

region). The estimates for the Big Bend area are highly uncertain due to limited data. The results are summarized in **Table 4** and illustrated in **Figure 19**.

Table 4 Monte Carlo HIP-RA results for 2,500 iterations

A) Results from Monte Carlo simulations of heat output (in MW)

Zone	Region	Producible Heat × 10^{17} (MW)	Producible Heat/ Unit Area × 10^{13} (MW/km^2)	Producible Heat/ Unit Volume × 10^{13} (MW/km^3)
Basement	Big Bend	0.84	5.76	9.20
Basement	Warm	3.57	5.73	9.20
Basement	Hot	1.15	5.04	8.04
PzMz	Big Bend	0.48	3.27	5.30
PzMz	Warm	2.11	3.38	5.33
PzMz	Hot	0.36	1.59	2.52
Tertiary	Big Bend	0.02	0.11	0.18
Tertiary	Warm	0.07	0.11	0.17
Tertiary	Hot	0.02	0.11	0.17

QAe9951

B) Results from Monte Carlo simulations of electricity output (in MW)

Zone	Region	Producible Electricity (MW)	Producible Electricity/ Unit Area (MW/km^2)	Producible Electricity/ Unit Volume (MW/km^3)
Basement	Big Bend	53,853.71	36.88	58.92
Basement	Warm	229,243.37	36.73	58.93
Basement	Hot	73,900.71	32.26	51.53
PzMz	Big Bend	28,714.16	19.66	31.91
PzMz	Warm	126,898.22	20.33	32.09
PzMz	Hot	18,057.57	7.88	12.51
Tertiary	Big Bend	304.97	0.21	0.34
Tertiary	Warm	1,304.36	0.21	0.33
Tertiary	Hot	470.95	0.21	0.32

QAe9951

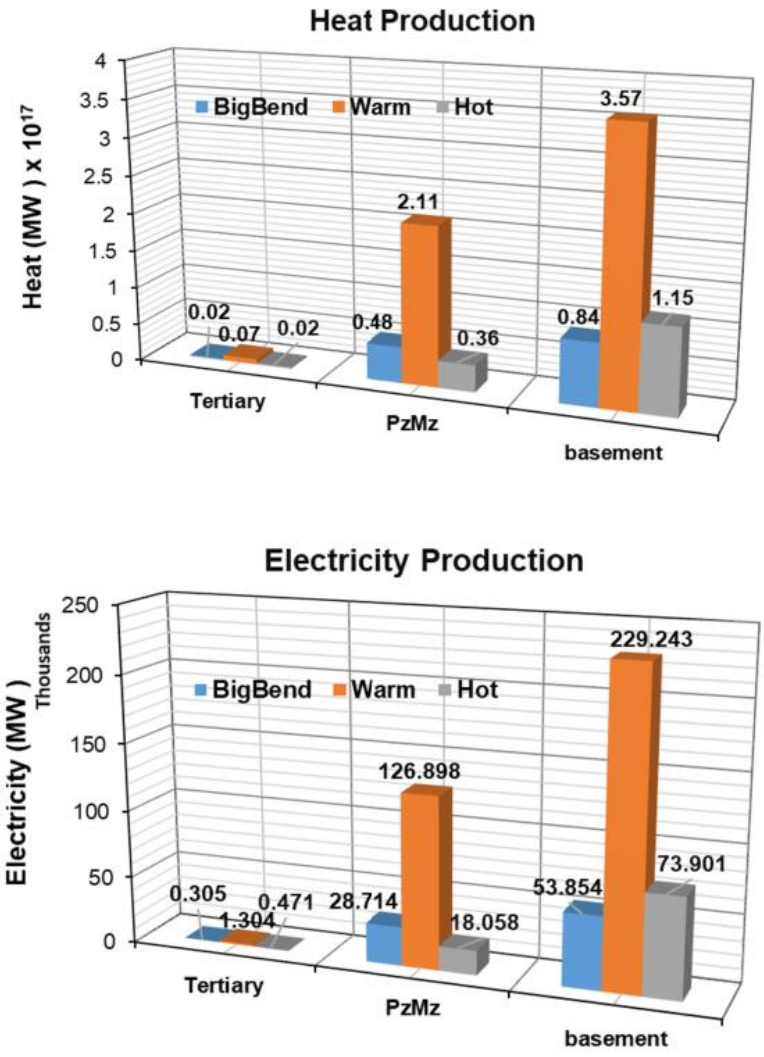

Figure 19. Estimated producible heat and electricity (units are in MW) for three reservoirs in Big Bend, Warm (Interior), and Hot (Border) regions using Monte Carlo HIP-RA analysis (Wisian et al., 2024).

The HIP-RA findings demonstrate comparable results across various zones, revealing observable and justifiable variations. Certain areas within the Border Region exhibit the shallowest and hottest reservoirs, indicating a higher potential for electricity generation, compared to the Interior and Big Bend regions. Despite these differences, the basement reservoir temperature

remains relatively similar across all zones, resulting in comparable estimates of producible heat and electricity levels in each region. This consistency is primarily due to the greater depth of reservoirs in the Interior regions compared to similar temperature reservoirs found in portions of the Border region.

Given that drilling costs can account for nearly half of a project's total expenses, shallower reservoirs present a more economically viable option. Consequently, the cost-effectiveness of the basement reservoir in the Border region surpasses that of similar reservoirs in the Big Bend and Interior regions. It is essential to clarify that economic considerations are not part of the HIP-RA analysis, so this distinction is not apparent in the results presented in **Table 4**. For further insights on how target drilling depth influences economics, please refer to the GEOPHIRES findings below.

GEOPHIRES project scenarios

The GEOPHIRES project results focus on specific project scenarios rather than regional-level analyses from HIP-RA. In this study, we modeled a variety of potential scenarios, including four models for electricity production (**Table 5**) and four models for direct use or hybrid applications (**Table 6**). We identified a significant opportunity to develop a scenario for the Border Region's Precambrian Basement Reservoir by employing a conventional hydrothermal approach that leverages the known Chinati Hot Springs. However, we opted not to model this scenario at this stage, as further detailed research into the characteristics of the hot springs is necessary. It is important to note that we do not have any techno-economic feasibility study for the Big Bend region due to a lack of reliable data from that area.

It is essential to highlight that the estimates presented do not incorporate local or state subsidies, though these subsidies could represent a significant financial benefit. These credits can significantly affect project viability; it can turn a marginally economically viable project into a fully viable one (see scenario 3 for details). We included the federal Inflation Reduction Act (IRA), which offers both Investment Tax Credits (ITC) and Production Tax Credits (PTC) in this study.

In all scenarios, we have used a 50% IRA Investment Tax Credit, as such credits are increasingly prevalent. However, it remains unclear how a PTC credit would apply to a non-taxable entity that produces and consumes its energy "behind the fence." Furthermore, as of the submission date of this paper, there has been no determination regarding how direct-use projects may qualify for an ITC or PTC.

It is important to note that these techno-economic analyses are conservative with various assumptions. This is a dynamic field due to various factors, including supply chain, co-production of fluids, newer heat extraction technologies, etc., which could change the overall economic picture.

GEOPHIRES electricity generation models:

The financial model assumes electricity will be sold at a price starting at 15 cents/kWh and increasing by 2% annually due to inflation. **Table 5** summarizes the results from four electricity generation scenarios.

1) Border Region, Precambrian basement reservoir, EGS style, with a maximum initial reservoir temperature of 240°C (aspirational) – This scenario is believed to produce the most electricity

at the lowest cost for all of Presidio County. Therefore, efforts were made to maximize electricity production in this optimal scenario. It assumes the plant will be located near Presidio, drilling into the basement reservoir in the Border zone, close to existing transmission lines. The location may integrate with existing facilities, such as NAS Battery and the Acacia Solar Plant. The plan will involve drilling four wells (two injectors and two producers) to a total depth of 4.7 kilometers and constructing an energy production plant with a 30-year lifespan, for a total system cost of $57.08 million (after the Investment Tax Credit). The annualized capital cost is $2.85 million, and the operating cost is $3.2 million. The plant is projected to produce an average of 20.83 MW from an initial reservoir temperature of 241.7°C. The Levelized Cost of Energy (LCOE) for the project is $0.0371 per kWh, with a net present value (NPV) of $316.75 million, an internal rate of return (IRR) of 40.98%, and a multiple on invested capital (MOIC) of 5.5.

2) Border Region, Precambrian basement reservoir, EGS style, with a maximum initial reservoir temperature of 200°C. This scenario assumes a more achievable project today, requiring no new technologies. It is identical to Scenario 1, except the modeled reservoir temperature is approximately 200°C. The wells will be drilled to a depth of 3.7 kilometers in the Precambrian basement reservoir in the Border Region, near existing transmission lines and potentially integrated with NAS Battery and the Acacia Solar Plant. This plan also involves drilling four wells (two producers and two injectors). The total system cost is estimated to be $39.98 million (after ITC, which is lower than Scenario 1 due to shallower wells), with an annualized capital cost of $2 million and an operating cost of $2.43 million. The geothermal plant is expected to produce 12.25 MW from an initial reservoir temperature of 196.7°C. The LCOE is $0.0461

per kWh, and the project has an NPV of $173.43 million, an IRR of 33.92%, a VIR of 5.34, and a MOIC of 4.18.

3) Border Region, Precambrian basement reservoir, AGS/CLGS style (Yuan, 2021))– This scenario explores a different geothermal approach, utilizing AGS with a CLGS. All inputs remain the same as Scenario 2, but it is important to note that AGS projects have considerable uncertainties regarding drilling costs.

4) Interior Region, Precambrian basement reservoir, AGS/CLGS style – This scenario envisions a power plant located near the ERCOT transmission lines in the Marfa area or directly connected to the Permian Basin to support hydrocarbon production. It follows the same style as Scenario 3, but with a target temperature that is 25°C lower.

Table 5: Summary of electricity generation scenarios in Border and Interior regions (Wisian et al., 2024).

Scenario	Style	Region	Reservoir	Electricity (MW)	LCOE (cents/kWh)	NPV (M$)	IRR (%)	VIR=PI=PIR	Temperature (°C)	CAPEX (M$)	OPEX (M$)
1	EGS (250)	Border	Basement	20.83	3.71	316.75	40.98	6.55	241.7	57.08	3.2
2	EGS (200)	Border	Basement	12.25	4.61	173.43	33.92	5.34	196.7	39.98	2.43
3	AGS (200)	Border	Basement	5.54	13.53	7.32	7.07	1.1	173	71.24	2.3
4	AGS (175)	Interior	Basement	5.46	15.28	-6.35	5.6	0.92	172	80.78	2.48

Direct-use/hybrid models

The financial model assumes an initial sale price for heat at 12 cents/kWh, increasing by 2% annually due to inflation after the plant's completion. If cooling is involved, the pricing model mirrors that of electricity. Additionally, the model includes a fixed credit of $0.039 per pound of CO_2 saved when using carbon credit (Wisian et al., 2024). **Table 6** summarizes the results from four direct use scenarios.

5) Border Region, PzMz reservoir, Agri-food processing plant, with a targeted heat production temperature of 240°C – This 30-year scenario is quite similar to Scenario 6, envisioning a food processing plant in Presidio City near the Texas-Pacifico South Orient Rail Line, where all the heat generated is utilized in food processing activities requiring heat, such as fruit drying. The simple two-well fractured system is drilled to a depth of 4.7 km and produces water at 238.4°C and a flow rate of 55 kg/sec. Over the project's lifetime, the system produces an average of 37.45 MW of heat at a cost of $2.72 per MMBTU. The capital expenditure (CAPEX) for the geothermal system is about $23.3 million, with an operating expense (OPEX) of $1.56 million, resulting in an NPV of $558.91 million, an IRR of 147.29%, a VIR equal to the profit-investment ratio (PI=PIR) of 24.97, and a MOIC of 20.54.

6) Interior Region, PzMz reservoir, Combined Heat and Power (CHP) for a greenhouse complex for food/ crop production – This 30-year scenario envisions a minimal 2-well fractured geothermal system located in the PzMz reservoir of the Marfa region, coupled with a greenhouse complex for food and high-value crop production. This system is similar to scenario 5, but it provides both heat and electricity. The heat is utilized directly in the greenhouse to promote optimal plant growth and can also be converted to cooling using an

absorption chiller if necessary. Wells are drilled into the PzMz reservoir to a depth of 3.1 km, producing water at approximately 100°C. The system equally splits this water between generating electricity via a subcritical Organic Rankine Cycle (ORC) generator and heating (or cooling) the greenhouse. The electricity generation capacity is about 0.069 MW, with the heat/cooling system supplying around 2.8 MW, produced at a cost of US$4.30/MMBTU. The total capital expenditure (CAPEX) for the geothermal portion of this project, excluding the greenhouse itself, is estimated at US$8.93 million, with an annual operating expense (OPEX) of US$0.42 million. Financial projections indicate a net present value (NPV) of US$32.9 million, an internal rate of return (IRR) of 29.89%, a value investment ratio (VIR) equivalent to the profitability index (PI) and profitability index ratio (PIR) of 4.68, and a multiple on invested capital (MOIC) of 4.3.

7) Interior Region, Precambrian basement reservoir, geothermally powered Direct Air Capture of CO_2 using a solid sorbent method (S-DAC-GT, (Kuru, 2023)) – In this scenario, a geothermal system is paired with a newly constructed plant that captures CO_2 from the atmosphere using a solid sorbent method (S-DAC-GT, Kuru, 2023). The captured CO_2 is either delivered to the greenhouse from scenario 1 to enhance agricultural productivity or sold in the Permian Basin for enhanced oil recovery processes. The plant may qualify for federal credits for carbon capture and use, although estimates for these credits are outside the scope of this project. The GEOPHIRES model assumes an EGS-style completion in a deep reservoir (mostly, Precambrian basement) at a depth of 7 km, where it predicts an initial reservoir temperature of 222°C. The project anticipates an average lifespan of 20 years, but this may be an underestimation given the percentage of heat extracted from the site (~49%). Geothermal heat

is used to generate 12.1 MW of electricity and 4.82 MW of heat. The predicted capital cost for the geothermal component is about US$39.82 million, with an annual operating cost of US$2.27 million. The levelized cost of electricity (LCOE) for the surplus electricity is $0.0611/kWh, indicating that the project is unlikely to be profitable from electricity sales, which is not its primary purpose. The model estimates the cost of carbon extraction at $310.96 per tonne, capturing approximately 203,863,767 tonnes of CO_2 over the project's 20-year lifespan at a price of about $237.98 per tonne. For the project to be considered successful, purchasers of CO_2 must be willing to pay more than $237.98 per tonne, excluding any credits for carbon capture and use.

8) Interior Region, PzMz Reservoir, Absorption Chiller for commercial or industrial cooling – This scenario considers a customer focused solely on environmental cooling provided by an absorption chiller. Potential customers could include large office buildings or data centers. The input parameters are similar to those in scenario 2 (depth, number of wells, etc.), but 100% of the geothermal energy is dedicated to chilling, with an efficiency conversion greater than 75%. The lower economic performance in scenarios 2 and 3 is primarily due to the significant energy loss during electricity generation, where less than 15% of the heat energy is converted to electricity.

Table 6: Summary of the direct-use and combined-use scenarios (Wisian et al., 2024).

Scenario	Type of Direct use	Depth (km)	Temperature (°C)	NPV (M$)	IRR (%)	VIR=PI=PIR	Payback (years)	Lifetime (years)	Heat (MW)	CAPEX (M$)	OPEX (M$)
5	Agri-processing	4.7	238.4	558.61	147.29	24.97	1.69	30	37.45	23.3	1.56
6	Greenhouses	3.1	100.2	32.9	29.89	4.68	4.54	30	2.8	8.93	0.42
7	Geothermally driven DAC	7	222	29.42	13.81	1.74	8.05	20	4.82	39.82	2.27
8	Absorption chiller	6	209	241.05	90.3	11.71	2.13	20	27.31	22.51	1.26

It is important to note that the NPV for both the greenhouse and CO_2 capture scenarios may be low or negative, suggesting they would typically be considered marginally economic. However, in both cases, the sales of heat and/or electricity are not the primary sources of revenue. Instead, these projects facilitate operations that generate revenue—greenhouses cultivate food for sale, while CO_2 capture can yield income from credits associated with carbon capture and utilization. The net costs of these geothermal activities represent only a portion of the overall expenses involved in generating revenue.

These scenarios represent just a small subset of potential opportunities in the study area. While some projects show promising financial prospects, others may face challenges and require innovative and collaborative strategies. Government incentives could significantly affect the economic viability of these initiatives, and projects may combine different revenue streams.

The Texas-Pacifico South Orient Rail Line (TP-SORL) International Inspection Station is projected to be completed by the summer of 2025, enabling international freight to flow through Presidio County (Karas, 2022; Karas, 2023). Should affordable geothermal heat become accessible near the TP-SORL, agricultural suppliers could leverage this resource to process their food, significantly enhancing the value of their products and facilitating access to larger international

markets, such as Mexico (Wisian et al., 2024). This shift of industry closer to consumers exemplifies the trend of nearshoring.

Grid, Local Electricity Generation, Economic Development Zone, and Value of Geothermal in the study area

Presently, Presidio County does not have any electric generation facilities and relies solely on a single ERCOT transmission line that connects Presidio City to Marfa (see Figure 2). It is crucial to upgrade the electric service capacity and reliability to foster economic growth in Presidio County. One key benefit of developing geothermal electricity production in Presidio County is the potential to provide local baseload generation, which would be available around the clock for immediate economic development use.

Presidio City already features a solar facility that sells energy to Bryan Texas Utilities, alongside a 4 MW molten sodium-sulfur (NAS) battery installation. The introduction of geothermal energy could significantly enhance the resilience of the electrical supply, especially in the face of increasing severe weather and drought conditions in the Trans-Pecos region.

A significant portion of Presidio County is designated as a state Economic Development Zone (EDZ), which encompasses nearly half of the border region, including the entirety of Presidio City. This area has a strong demand for energy and an existing renewable energy infrastructure. The EDZ offers capital gains tax abatements for investments in eligible zone assets. Consequently, a geothermal project that strengthens the existing renewable energy framework could be both advantageous and eligible for considerable subsidies.

We also performed a high-level assessment of carbon savings by replacing natural gas with geothermal energy for electricity generation in the study area, assuming complete methane combustion without carbon capture. Annual CO_2 reductions were calculated for different energy outputs, indicating that generating 0.32 MW could avoid approximately 1,093,000 kg of CO_2 emissions annually, while 58.93 MW could save up to 201,353,000 kg. These results highlight geothermal energy's significant potential for reducing greenhouse gas emissions and promoting sustainable energy solutions.

Moreover, there is a prospective opportunity for establishing a grid connection across the international border between the US and Mexico. However, this study does not explore that aspect. The establishment of a geothermal heat processing operation in the study area represents a promising opportunity for nearshoring.

Next Steps/Recommendations

This study uses an integrated workflow for subsurface characterization and techno-economic feasibility analysis of geothermally driven electricity generation and direct-use at a sub-county scale resolution under various data limitations, uncertainties, and assumptions. The study does not offer sufficient resolution to pinpoint specific sites for economically viable drilling projects.

To enhance our understanding and further reduce risks and uncertainties, additional work is recommended. This includes drilling and temperature logging, coring wells, conducting a detailed assessment of local hydrology, obtaining high-resolution geophysical surveys and

chemical assays from local hot springs, measuring thermal conductivity under subsurface conditions, and updating techno-economic models.

Conclusions

We have developed and demonstrated an integrated workflow for subsurface characterization, resource estimation, and techno-economics in a geologically complex area with limited data. Presidio County, located in the Trans-Pecos region of Texas, has substantial undeveloped geothermal resources, referred to as HIP-RA. These resources could be economically viable for various applications, including electricity production, industrial uses, and heating and cooling.

Using literature, high-resolution gravity data tied to deep boreholes, we have identified the presence of multiple basins and structures in the study area: Valentine Basin, Marfa Basin, Presidio Bolson, and Redford Bolson. These basins display varied structures and a highly irregular Precambrian basement, with depths ranging from 0 (surface) to 6 km.

Most faults in the study area are extensional in nature, related to the Rio Grande Rift and trending NW-SE. We have identified newer faults, particularly near Valentine Basin and Presidio City, in the deep subsurface by utilizing high-resolution gravity data and tilt derivative maps. We recommend further geophysical exploration to validate these faults.

Deep reservoirs, such as the Ellenburger Group, are highly fractured. Both breccia (older, irregular in shape, and numerous) and tectonic-related fractures (younger, sub-vertical, and in opening mode) are present in the core. Many of the brecciated zones are mineralized, indicating these rocks can be stimulated. However, care must be taken to avoid rapid heat flow paths through

these highly complex and interconnected fractures in Enhanced Geothermal Systems (EGS) to reduce the risk of rapid production decline.

The Border region boasts a high geothermal gradient (~47°C/km) compared to the interior region (~29°C/km), which makes it very promising for geothermal project development. Although the Interior region is cooler than the Border region, it still represents an excellent geothermal resource and is comparable to many sedimentary basins worldwide.

The southeast corner of the county, known as the Big Bend Region, remains under-explored due to a lack of data beyond surface geological mapping. As a result, its potential remains largely unknown.

Based on our current techno-economic modeling in GEOPHIRES with underlying assumptions, we believe sufficient electricity generation (in the order of tens of megawatts) is feasible, with a profitable Levelized Cost of Electricity (LCOE) less than the selling price of the electricity to the grid. The projections show a high Net Present Value (NPV) and a short payback period if EGS wells are completed in the basement of the border region, targeting temperatures of at least 200°C or more.

Regarding direct-use applications, agricultural processing and absorption chillers show promise, offering a high NPV, high Internal Rate of Return (IRR), and short payback periods. We anticipate that these findings will evolve with advancements in technology and additional subsurface information from further exploration.

Acknowledgements

This research was funded by the Presidio Municipal Development District and with support from the State of Texas Advanced Resource Recovery geothermal program. The authors thank Trey Gerfers, General Manager, Presidio County Underground Water Conservation District for his work in making this study possible. We thank Getech for the provision of their proprietary gravity data over the study area. We thank Seequent for donating Oasis Montaj™ software to the University of Texas at Austin.

References

Barker, D. S. (1977). Northern Trans-Pecos magmatic province: Introduction and comparison with the Kenya rift. Geological Society of America Bulletin, 88(10), 1421-1427.

Bankey, V. (2006). Texas magnetic and gravity maps and data: A website for distribution of data (No. 232). US Geological Survey.

Batir, J., and Richards, M. (2020). *Analysis of Geothermal Resources in Three Texas Counties.* Dallas.

Beckers, K. F. (2019). GEOPHIRES v2. 0: updated geothermal techno-economic simulation tool. *Geothermal Energy*, 1-28.

Blackwell, D. M. (2011). *Heat flow map of the continental U.S in 2011*. Retrieved 1 28, 2024, from SMU Geothermal Lab: https://www.smu.edu/-/media/Site/Dedman/Academics/Programs/Geothermal-Lab/Graphics/SMUHeatFlowMap2011_CopyrightVA0001377160_jpg.jpg

Blakely, R. J. (1996). Potential theory in gravity and magnetic applications. Cambridge university press.

Davies, J. D. (2010). Earth's surface heat flux. *Solid Earth, 1*(1), 5-24.

Dietrich, J. W. (1965). *Geology of Presidio Area, Presidio County, Texas.* The University of Texas at Austin.

Electric Reliability Council of Texas. (2024, Jan 30). *Fuel Mix*. Retrieved from ercot: https://www.ercot.com/gridmktinfo/dashboards/fuelmix

Electric Transmission Texas. (2020). *Summary of Presidio Battery Operations for 2020*. Retrieved from ETT: http://ettexas.com/Content/documents/2020SummaryofPresidioBattery.pdf

Electric Transmission Texas. (n.d.). *Presidio NaS Battery Project*. Retrieved from Project and Plans: http://www.ettexas.com/Projects/Presidio

Federal Reserve Bank of Saint Louis. (2023). *Unemployment Rate in Presidio County, TX*. Retrieved 01 02, 2024, from FRED Economic Data: https://fred.stlouisfed.org/series/LAUCN483770000000003A

Finger, D. C., Saevarsdottir, G., and Svavarsson, H. G. (2021). Improved Value Generation from Residual Resources in Iceland: the First Step Towards a Circular Economy. *Circular Economy and Sustainability, 1*, 525-543. doi:10.1007/s43615-021-00010-7

Stefanie Naoko Frelinger, S.N. (2015). Chronology of Laramide Magmatism and Stockwork Fracture Filling at the Red Hills Porphyry Mo-Cu Deposit, Presidio County, Texas, The University of Texas at Austin, MS Thesis.

Gale, J.F. and Gomez, L.A., 2007, Late opening-mode fractures in karst-brecciated dolostones of the Lower Ordovician Ellenburger Group, west Texas: Recognition, characterization, and implications for fluid flow. *AAPG bulletin, 91*(7), p.1005-1023.

Garg, S. K.and Combs, J., (2011). A reexamination of USGS volumetric "Heat in Place" method. *Proceedings*. Thirty-Sixth Workshop on Geothermal Reservoir Engineering Stanford University, Stanford

Goldich, S. and. (1949). Stratigraphy and petrology of the Buck Hill quadrangle, Texas. *Geological Society of America Bulletin,* 1133-1182.

Harrison W. E., L. K. (1983). *Geothermal resource assessment of Oklahoma.* Oklahoma Geologic Survey.

Henry, C, D. (1979a). Crustal structure deduced from geothermal studies, Trans-Pecos Texas, in Walton, A. W., and Henry, c. d., eds., Cenozoic geology of the Trans-Pecos volcanic field of Texas: The University of Texas at Austin, Bureau of Eocnomic Geology Guidebook 19, p. 39-47.

Henry, C. D. and Muehlberger, W. R. (1996). Geology of the Solitario Dome, Trans-Pecos Texas: Paleozoic, Mesozoic, and Cenozoic Sedimentation, Tectonism, and Magmatism. 182 p., doi.org/10.23867/RI0240D/RI0240D

Hittleman, A.D., Dater, D., Buhmann, R., and Racey, S., 1994, Gravity CD-ROM and Users's Manual (1994 ed.): National Oceanic and Atmospheric Administration, National Geophysical Data Center, Boulder, Colorado.

Karas, S. (2022, December 7). *TxDOT projects December 2024 completion date for Presidio rail inspection facility*. Retrieved from The Big Bend Sentinel: https://bigbendsentinel.com/2022/12/07/txdot-projects-december-2024-completion-date-for-presidio-rail-inspection-facility/

Kerans, Charles, 1989, Karst-controlled reservoir heterogeneity and an example from the Ellenburger Group (Lower Ordovician) of West Texas: *The University of Texas at Austin, Bureau of Economic Geology Report of Investigations No. 186*, 40 p.

Kerans, Charles, 1990, Depositional systems and karst geology of the Ellenburger Group (Lower Ordovician), subsurface West Texas: *The University of Texas at Austin, Bureau of Economic Geology Report of Investigations No. 193*, 63 p., 6 pl.

Kucks, R. P., (1999). Bouguer gravity anomaly data grid for the conterminous US

Henry, C, D. (1998). "Geology of Big Bend Ranch State Park, Texas." Guidebook - Bureau Of Economic Geology, University Of Texas At Austin.

Henry, C. D. (1979b). Geologic setting and geochemistry of thermal water and geothermal assessment, Trans-Pecos Texas, with tectonic map of the Rio Grande area, Trans-Pecos Texas and adjacent Mexico.

Keller, G. R., Hinze, W. J., Aiken, C. L. V., Goodell, P. C., Roy, R. F., and Pingitore, N. E. (1981). Evaluation and combined geophysical interpretations of NURE and related geoscience data in the Van Horn, Pecos, Marfa, Fort Stockton, Presidido, and Emory Peak quadrangles, Texas. Volume 1. Final report (No. GJBX-365-81). Bendix Field Engineering Corp., Grand Junction, CO (United States); Texas Univ., El Paso (USA). Dept. of Geological Sciences.

Kopp, R. A. (1977). *Geothermal exploration of Presidio County, Texas.* The University of Texas at El Paso.

Kuru, T. K. (2023). Solid sorbent direct air capture using geothermal energy resources (S-DAC-GT)–Region specific analysis. *Geoenergy Science and Engineering*, 211645.

Lear, J., Bennett, C., and 10 others, 2016, El Paso County Geothermal Project at Ft. Bliss, Final Project Report for DOE Contract DE-EE0002827, 160 p. with appendixes.

Loucks, R. G., 1999, Paleocave carbonate reservoirs: origins, burial-depth modifications, spatial complexity, and reservoir implications: AAPG Bulletin, v. 83, p. 1795–1834.

Loucks, R. G., and Anderson, J. H., 1985, Depositional facies, diagenetic terrains, and porosity development in Lower Ordovician Ellenburger Dolomite, Puckett Field, West Texas, *in* Roehl, P. O., and Choquette, P. W., eds., *Carbonate petroleum reservoirs: Springer-Verlag*, p. 19–38.

Lonsdale, J. T. (1940). Igneous rocks of the Terlingua-Solitario region, Texas. *Bulletin of the Geological Society of America*, 1539-1626.

Lowry, T. F. (2019). GeoVision Analysis Supporting Task Force Report: Reservoir Maintenance and Development. *Lowry, T., Finger, J., Carrigan, C., Foris, A., Kennedy, M., Corbet, T., ... and Sonnenthal, E. (2017). GeoVision Analysis Supporting Task ForcSAND2017-9977. Albuquerque, NM: Sandia National Laboratories*.

Miggins, D.P., Ren, M., Anthony, E.Y., 2008. Volcanic geology of several prominent outcrops in the western part of Big Bend National Park. In: Gray, J.E., Page, W.R. (Eds.), Geological, Geochemical and Geophysical Studies by the U.S. Geological Survey in Big Bend National Park, Texas, pp. 29–42.

Miller, H. G., and Singh, V. (1994). Potential field tilt—a new concept for location of potential field sources. Journal of applied Geophysics, 32(2-3), 213-217.

Mraz, J. a. (1980). *Structure of the Presidio bolson area, Texas, interpreted from gravity data.* Bureau of Economic Geology, Univ. of Texas at Austin.

Muffler, P. and Cataldi, R. (1978). Methods for regional assessment of geothermal resources. *Geothermics,* 53-89.

O'Donnell Jr, T.M., Miller, K.C., and Witcher, J.C. (2001) A seismic and gravity study of the McGregor geothermal system, southern New Mexico. *Geophysics*, 66(4), 1002-1014.

Parker, D. F., Ren, M., Adams, D. T., Tsai, H., and Long, L. E. (2012). Mid-Tertiary magmatism in western Big Bend National Park, Texas, USA: evolution of basaltic source regions and generation of peralkaline rhyolite. Lithos, 144, 161-176

Parry, C. (1857). *Report on the United States and Mexican boundary survey, Part 2, Paleontology and Geology of the Boundary.* Dept. of Interior.

Rix, C. C., 1953, Geology map of Chinati Peak Quadrangle, Presidio County, Texas (preliminary edition): University of Texas, Austin, Bureau of Economic Geology Miscellaneous Map 4, scale 1:48,000.

Roest, W. R., Verhoef, J., and Pilkington, M. (1992). Magnetic interpretation using the 3-D analytic signal. Geophysics, 57(1), 116-125.

Salem, A., Williams, S., Fairhead, D., Smith, R., and Ravat, D. (2008). Interpretation of magnetic data using tilt-angle derivatives. Geophysics, 73(1), L1-L10.

Stoeser, D.B., Shock, N., Green, G.N., Dumonceaux, G.M., and Heran, W.D. (1992), Geologic map of Texas, Southwest Quadrant, Data Series 170 Plate 3 Version 1.1, https://pubs.usgs.gov/ds/2005/170/downloads/pdf/Texas_SW_Quadrant.pdf

Talwani, M., Worzel, J. L., and Landisman, M. (1959). Rapid gravity computations for two-dimensional bodies with application to the Mendocino submarine fracture zone. Journal of Geophysical Research, 64(1), 49–59

TxDOT Rail Divison. (2022). *2022 South Orient Rail Line Annual Report.* Texas Department of Transportation. Retrieved from https://ftp.txdot.gov/pub/txdot/move-texas-freight/2022-south-orient-rail-annual-report.pdf

USGS, (2020). Quaternary Fault and Fold Database for the Nation. https://doi.org/10.5066/P9BCVRCK

United States Census Bureau. (2020). *Presidio County, Texas*. Retrieved 01 02, 2024, from data.census.gov: https://data.census.gov/profile?g=050XX00US48377

West Texas Economic Development District. (2021). *Economic Development*. Retrieved 01 02, 2024, from Rio Grande Council of Governments: http://www.riocog.org/wp-content/uploads/2022/09/2021thru2025.WTEDD_.CEDS_.pdf

Walton A.W., and Henry, C.D., 1979, Cenozoic Geology of the Trans-Pecos Volcanic Field of Texas, Bureau of Economic Geology, Guidebook 19.

Wisian, K., Ross, M., Bhattacharya, S., Khaled, M., Young, B., Chapman, D., and Turan, A., 2024, Presidio County Geothermal Assessment, A report submitted to the Presidio Municipal Development District,

https://www.co.presidio.tx.us/upload/page/4648/2024/presidio_county_geothermal_assessment_final_v2.pdf

Yuan, W. C. (2021). Closed-loop geothermal energy recovery from deep high enthalpy systems. *Renewable Energy*, 976-991.